

CONSTRAINTS IN COSMOLOGICAL PARAMETER SPACE FROM
THE SUNYAEV-ZEL'DOVICH EFFECT AND
THERMAL BREMSSTRAHLUNG

S. M. MOLNAR^{1,2}, M. BIRKINSHAW³, AND R. F. MUSHOTZKY¹

Draft version November 6, 2018

ABSTRACT

We discuss how the space of possible cosmological parameters is constrained by the angular diameter distance function, $D_A(z)$, as measured using the SZ/X-ray method which combines Sunyaev-Zel'dovich (SZ) effect and X-ray brightness data for clusters of galaxies. New X-ray satellites, and ground-based interferometers dedicated to SZ observations, should soon lead to $D_A(z)$ measurements limited by systematic rather than random error. We analyze the systematic and random error budgets to make a realistic estimate of the accuracy achievable in the determination of $(\Omega_m, \Omega_\Lambda, h)$, the density parameters of matter and cosmological constant, and the dimensionless Hubble constant, using $D_A(z)$ derived from the SZ/X-ray method, and the position of the first ‘‘Doppler’’ peak in the cosmic microwave background fluctuations. We briefly study the effect of systematic errors. We find that Ω_m , Ω_Λ , and w are affected, but h is not by systematic errors which grow with redshift. With as few as 70 clusters, each providing a measurement of $D_A(z)$ with a 7% random and 5% systematic error, Ω_m can be constrained to ± 0.2 , Ω_Λ to ± 0.2 , and h to ± 0.11 (all at 3σ). We also estimate constraints for the alternative three-parameter set (Ω_m, w, h) , where w is the equation of state parameter. The measurement of $D_A(z)$ provides constraints complementary to those from the number density of clusters in redshift space. A sample of 70 clusters (D_A measured with the same accuracy as before) combined with cluster evolution results (or a known matter density), can constrain w within ± 0.45 (at 3σ). Studies of X-ray and SZ properties of clusters of galaxies promise an independent and powerful test for cosmological parameters.

1. INTRODUCTION

What set of cosmological parameters characterizes our Universe?

According to the most popular cold dark matter (CDM) scenario, the Universe consists of baryonic matter and a substantial amount of ‘‘dark’’ matter. A variety of recent measurements have led to the conclusion that the matter density parameter $\Omega_m \approx 0.3$ (Turner 2000), while CMB measurements strongly favor a flat space time (Bernardis et al. 2001; Lee et al. 2001), and SNe Ia measurements indicate that the Universe is accelerating, suggesting a negative pressure (Riess et al. 2000; Perlmutter et al. 1999). Taken together, these pieces of evidence suggest that the baryonic and dark matter content of the Universe is supplemented by an additional smooth component with negative pressure, P_w , modeled by the equation of state $\rho_w c^2 = -w P_w$, where ρ_w is the density of this component, w is a dimensionless state parameter of order unity (cf. Huterer & Turner 2000).

Each existing dataset constrains, with limited accuracy, some subset of the cosmological parameters. Different measurements and combinations of measurements, such as SNe Ia, Cosmic Microwave Background (CMB) fluctuations, IRAS infrared galaxy surveys, classical double radio galaxy properties, 1.2-Jy galaxy redshift surveys, gravitational lensing, cluster X-ray temperature function and cluster number counts, baryon and gas mass fraction, and the SZ effect have been used to constrain cosmological pa-

rameters (Jaffe et al. 2000; Balbi et al. 2000; Tegmark & Zaldarriaga 2000; Guerra, Daly & Wan 2000; Efstathiou et al. 1999; Lasenby et al. 1999; Perlmutter et al. 1999; Gawiser & Silk 1998; Lineweaver 1998; White 1998; Pen 1997; Sasaki 1996; Huterer & Turner 2000; Majumdar & Subrahmanyam 2000; Bridle et al. 1999; Diego et al. 2001).

In the future, the SNAP project (<http://snap.lbl.gov>) plans to use the SNe Ia method to determine the matter density and the cosmological constant at the few percent level. Even with the next-generation CMB satellites, MAP and Planck, degeneracies will remain among the cosmological parameters that can be estimated from the results (Efstathiou & Bond 1999; Zaldarriaga, Spergel & Seljak 1997). The importance of using a wide range of methods, therefore, is twofold. First, a simultaneous consideration of all data sets should allow the best joint estimation of the cosmological parameters. Second, the agreement of different techniques for measuring the cosmological parameters should provide a cross-check of our understanding of the underlying processes and a control against systematic errors. As we extend our analysis of the CMB to more complicated models (tensor fluctuations, finite neutrino masses, etc.) the number of cosmological parameters increases, and it becomes even more important that the widest possible range of datasets is used, and that strong controls against systematic errors are in place.

Many of the techniques of cosmological parameter estimation use clusters as tracer particles. As a result there is

¹ NASA/Goddard Space Flight Center, Laboratory for High Energy Astrophysics, Greenbelt, MD 20771

² Present address: Department of Physics and Astronomy, Rutgers University, 136 Frelinghuysen Road, Piscataway, NJ 08854, sandorm@physics.rutgers.edu

³ Department of Physics, Bristol University, Tyndall Avenue, Bristol, BS8 1TL, UK

a large number of planned cluster surveys in the two most important non-optical observational indicators of clustering: the SZ effect and cluster X-ray emission. Sunyaev-Zel'dovich effect surveys with dedicated interferometers or receiver arrays will observe hundreds of clusters with $z > 0.5$ per year (Browne et al. 2000; Holder, Carlstrom & Mohr 2000; Bartlett 2000). The new X-ray missions (Chandra, XMM) will provide data on hundreds of clusters with high redshift through their deep and medium-deep surveys.

Cluster evolution, the redshift distribution of clusters from SZ and X-ray surveys, $N_{SZ}(z)$ and $N_X(z)$, and cluster number counts as a function of X-ray flux, $N_X(S)$, are important constraints on cosmological parameters. While methods based on the CMB power spectrum and SNe Ia are sensitive to the angular diameter distance, cluster evolution (and number counts) is sensitive to the growth function of matter density fluctuations. Bartlett (2000) estimated the performance of ground-based, arcminute-resolution, SZ surveys and concluded that more clusters will be detected with deep, small-area surveys than shallow, wide-area surveys. Kneissl et al. (2001) studied the performance of the Arcminute MicroKelvin Imager experiment and showed that a set of only about 20 clusters, with redshifts in the range $z = 0 - 0.8$ is needed to measure $N_{SZ}(z)$ sufficiently well to distinguish between $\Omega_m = 1$ and $\Omega_m = 0.3$ cosmologies. Carlstrom et al. (2001) discuss a deep SZ ground based survey, and quantify constraints from $N_{SZ}(z)$ on Ω_m and Ω_Λ . $N_{SZ}(S)$ and $N_{SZ}(z)$ were estimated from the proposed shallower, but all-sky Planck survey by Diego et al. (2001), who concluded that about 300 clusters (with the necessary optical follow-up to measure redshifts) would suffice to distinguish between open $\Omega_m = 0.3$ and flat $\Omega_m = 1$ cosmologies at 3σ confidence. Holder, Haiman & Mohr (2001) discussed the constraints on the parameter space defined by $(\Omega_m, \Omega_\Lambda, \sigma_8)$ (where σ_8 is the normalization of the matter power spectrum) using cluster evolution. Holder et al. showed that constraints from cluster evolution and SNe Ia observations are highly complementary to each other. Haiman et al. (2000) discussed the constraints on the (Ω_m, w, h) parameter space, assuming a spatially flat geometry ($\Omega_\Lambda = 1 - \Omega_m$), that follow from an SZ effect survey and a large angle deep X-ray survey (the Cosmology Explorer; Ricker and Lamb). They found that $N_{SZ}(z)$ and $N_X(z)$, combined with constraints from CMB or SNe Ia experiments, significantly reduce the degeneracies between Ω_m , w , and h . Huterer & Turner (2000) estimated the constraints on Ω_m and w for flat geometry that can be gained by combining results from SNAP, Planck and SZ and X-ray surveys.

As has been realized, the angular diameter distance-redshift relation, $D_A(z)$, is at the heart of many of these techniques, and is sensitive to some important combinations of cosmological parameters while being degenerate under others (Jaffe et al. 2000; Tegmark & Zaldarriaga 2000; Efstathiou et al. 1999; Lasenby et al. 1999; Perlmutter et al. 1999; White 1998). Recently White (1998) estimated constraints on the pairs of quantities $(\Omega_m, \Omega_\Lambda)$ and (Ω_m, w) (the latter in a flat Universe) from the $D_A(z)$ function based on current SNe Ia data combined with CMB first peak constraints. The analysis shows that the constraint on parameters based on $D_A(z)$ is nearly or-

thogonal to the constraint based on the position of the first peak in the CMB fluctuation spectrum. These two datasets are thus highly complementary, and form a particularly powerful pair of measurements (see also Tegmark et al. 1998).

The shape and normalization of the observed angular diameter distance function constrains several cosmological parameters (the standard formulae for distance in Friedmann-Robertson-Walker Universes are given in, for example, Peebles 1993). The distance - redshift function, $D_A(z)$, in CDM models depends on the matter density, cosmological constant and Hubble constant, and any other particle density which contributes to the curvature of space-time. The slope of the distance-redshift function at low redshift is a measure of the Hubble constant, while the shape of the function depends on the curvature and the different densities. In Figure 1 we show the fractional difference in $D_A(z)$ with fixed matter density and Hubble constant ($\Omega_m = 0.3$, $h = 0.65$), but various values cosmological constants ($\Omega_\Lambda = 0.7, 0.6, 0.3$, solid, dashed and dash dotted lines) relative to a model with zero cosmological constant ($\Omega_\Lambda = 0$). It can be seen from this figure, that $D_A(z)$ is most sensitive to the value of the cosmological constant at redshift about unity, and quite insensitive to that at small or high redshifts. In the redshift interval from $z = 0.5$ to $z = 1.8$ the angular diameter distance for flat ($\Omega_m = 0.3$, $\Omega_\Lambda = 0.7$) model is more than 10% different from a model with the same matter density but zero cosmological constant ($\Omega_m = 0.3$, $\Omega_\Lambda = 0$).

We can expect high precision data from hundreds of clusters of galaxies in the near future. With the present instrument suite, the statistical errors on individual measurements will be small, and so the usefulness of the data will be limited by their systematic errors. In this paper we evaluate the error budget of distance determination based on the SZ effect and X-ray measurements (assuming that the X-ray output is dominated by thermal bremsstrahlung, as is appropriate for the hot clusters in which the SZ effect is strong), and provide a realistic estimate of errors achievable in the angular diameter distance. We estimate how well one will be able to constrain the two parameter sets $(\Omega_m, \Omega_\Lambda, h)$, and (Ω_m, w, h) (assuming a spatially flat geometry, $\Omega_\Lambda = 1 - \Omega_m$) if this $D_A(z)$ function is combined with the position of the first Doppler peak in the angular power spectrum of CMB fluctuations.

Our treatment is complementary to previous work of Kneissl et al. (2001), Carlstrom et al. (2001), Diego et al. (2001), Holder et al. (2001), Haiman et al. (2000), and Huterer & Turner (2000), who used $N_{SZ}(z)$, $N_{SZ}(S)$, and $N_X(z)$ to constrain cosmological parameters, since we discuss the importance of $D_A(z)$. It also complements the work by White (1998), who used $D_A(z)$ determined from existing SNe Ia data to constrain $(\Omega_m, \Omega_\Lambda)$, and (Ω_m, w) (flat): the errors from the SZ/X-ray technique have significantly different characteristics, and we are concerned with the limitations that will be encountered with future survey data.

In the next section we briefly describe the well-known method of angular distance determination based on the SZ effect and thermal bremsstrahlung with an emphasis on how measurements are used, and how their error propagate to the angular diameter distance. In section 3 we

give a detailed analysis of the error budget, in section 4 we discuss the constraints on cosmological parameters. Finally, section 5 summarizes our conclusions.

2. DETERMINATION OF ANGULAR DIAMETER DISTANCE USING CLUSTERS

Distance determinations using the SZ effect and X-ray emission from the intra-cluster medium (SZ/X method hereafter) are based on the fact that these processes depend on different combinations of physical parameters of the clusters. The SZ effect (Sunyaev and Zel'dovich 1980; for recent reviews cf. Birkinshaw 1999, and Rephaeli 1995) is a result of inverse Compton scattering of CMB photons off hot electrons in the intra-cluster (IC) gas. The number of photons is conserved, but, on average, the photons gain energy, and thus generate a decrement in the Rayleigh-Jeans part of the spectrum and an increment in the Wien region. The amplitude of the SZ effect does not depend on the redshift of the cluster. We will discuss static thermal and kinematic thermal SZ effects in this paper, where the ‘‘static’’ effect is present in all clusters, and the ‘‘kinematic’’ effect is only present for those clusters with a non-zero line-of-sight (LOS) peculiar velocity relative to the Hubble flow. A typical Rayleigh-Jeans decrement of the static SZ effect is about about 50 times that of the kinematic SZ effect. The static SZ effect is proportional to the LOS pressure integral of the IC gas

$$\Delta T \propto g(\nu) \int dz n_e(\mathbf{r}) T_e(\mathbf{r}), \quad (1)$$

where $g(\nu)$ is the frequency dependence of the effect ($g \rightarrow -2$ in the non-relativistic Rayleigh-Jeans limit), and $n_e(\mathbf{r})$ and $T_e(\mathbf{r})$ are the electron density and temperature as functions of position within the cluster. The central X-ray surface brightness of a cluster is emission-weighted line-of-sight average of $n_e(z)^2 T_e(z)$:

$$S_X \propto \frac{1}{(1+z)^4} \int dz n_e(z)^2 T_e(z) \Lambda(T_e, Z_{ab}), \quad (2)$$

where $\Lambda(T_e, Z_{ab})$ is the cooling function integrated over the de-redshifted energy band of observations and Z_{ab} is the metal abundance of the gas.

On any given LOS, Equations 1 and 2, and the emission weighted X-ray temperature, \bar{T}_e (from spectroscopy), provide three independent integral constraints for the two functions, $n_e(\mathbf{r}_{LOS})$ and $T_e(\mathbf{r}_{LOS})$, although these functions cannot be determined uniquely. If, instead, one assumes parameterized functional forms for $n_e(\mathbf{r})$ and $T_e(\mathbf{r})$, these three equations can be used to constrain the controlling parameters. One important parameter that can be found from fitting the data is a characteristic LOS physical size of the system, R_{char}^{LOS} , and the angular diameter distance of the cluster can then be determined if this size is compared with the corresponding angular size, θ_{char}^{LOS} . However, we can measure only the apparent characteristic angular size, θ_{char}^{SKY} of the system as it appears projected into the plane of the sky (with corresponding physical size R_{char}^{SKY}). The main difficulty in the SZ/X method is the de-projection of the cluster from its 2-D images, that is the problem of finding the value of θ_{char}^{LOS} from the measured value θ_{char}^{SKY} . If this can be done, one can determine the angular diameter distance as

$$D_A = \frac{R_{char}^{LOS}}{\theta_{char}^{LOS}}, \quad (3)$$

If one assumes spherical symmetry, $\theta_{char}^{SKY} = \theta_{char}^{LOS}$, and a de-projection is possible without further assumptions about the functional forms of $n_e(\mathbf{r})$ and $T_e(\mathbf{r})$ (Silk & White 1978). This method, however, needs high signal/noise and high angular resolution SZ and X-ray images of the cluster, and thus the analytic de-projection has not been used so far. Most commonly, the distribution of gas in clusters is described by the spherical isothermal beta model (Cavaliere & Fusco-Femiano 1976). This model seems to give a good fit to X-ray data (Sarazin 1988), and thus it is usually assumed that the IC gas follows a spherical isothermal β model, where the IC gas is isothermal and in hydrostatic equilibrium in the gravitational potential of the cluster. The electron concentration in the cluster atmosphere is then $n_e(r) \propto (1+(r/r_c)^2)^{-3\beta/2}$, where r_c is the core radius (a suitable characteristic size of the cluster). The shape parameter β describes how the kinetic energy is distributed between the galaxies and IC gas. Typically $r_c = 0.1 h_{100}^{-1}$ Mpc, and $\beta \approx 2/3$ (Sarazin 1988). In practice, the IC gas temperature is determined from X-ray spectroscopy, the core radius projected in the plane of the sky, θ_c^{FIT} , and the shape parameter β^{FIT} are determined from fitting the β model to a high resolution X-ray image. Finally equations 1 and 2 are used to determine the angular diameter distance using Equation 3

$$D_A = \frac{r_c^{FIT}}{\theta_c^{FIT}} = \frac{r_c^{LOS}}{\theta_c^{LOS}}, \quad (4)$$

which is crucially dependent on the assumption of spherical symmetry: $r_c^{FIT} = r_c^{LOS}$.

If we adopt the beta model representation, we can write the angular diameter distance as a function of measurable quantities for a cluster as

$$D_A \propto \frac{1}{(1+z)^4} \frac{(\Delta T_0)^2}{S_{X0}(N_H)} \frac{\Lambda_e(T_e, Z_{ab})}{T_e^2} \frac{F(\beta)}{g^2(\nu) \theta_c}, \quad (5)$$

where ΔT_0 and S_{X0} are the central SZ effect and X-ray surface brightness (un-absorbed), N_H , is the absorbing column density, and $F(\beta)$ is a known function of β (or other parameters if a different description of the structure of the cluster is used). Some of the measured (or estimated) quantities on the RHS of this equation are highly correlated, so a careful error analysis is needed: the errors on individual quantities cannot be added in quadrature. No bootstrapping is required in using Eq. 5 (it is a direct method, with no need for using the usual cosmic distance ladder) as was realized by Sunyaev & Zel'dovich (1980), but the strong assumptions of spherical symmetry and isothermality are only crude approximations to the real situation.

It has been pointed out recently that relativistic effects become important for high temperature clusters (Rephaeli 1995). Relativistic corrections to the inverse Compton scattering have been calculated and used to interpret observations in terms of the Hubble constant (Rephaeli 1995; Birkinshaw 1999; Birkinshaw & Hughes 1998; Holzapfel et al. 1997, and references therein). Relativistic corrections to the thermal bremsstrahlung cooling function are also needed (Hughes & Birkinshaw 1998; Rephaeli & Yankovitch 1997). These corrections are in the order of 3% in D_A for high temperature ($T_e > 10$ keV) cluster. In this paper we assume that relativistic corrections have been made and we will not discuss their effect in detail.

3. ERROR BUDGET IN THE DETERMINATION OF THE ANGULAR DIAMETER DISTANCE

Errors in the determination of the angular diameter distance may be cast into two major categories: errors from measurements, and errors from theoretical modeling. Measurement errors can be statistical or systematic, while errors from theoretical modeling are systematic by nature. The systematic errors can be further classified as “random” or “non-random” depending on whether they average out or not for a statistical sample of clusters. In what follows we therefore use the expressions “random modeling errors” when discussing errors which introduce only scatter in the distance determination when averaged over an unbiased sample of clusters, and “non-random modeling errors” when discussing errors which introduce a bias in the distance determinations even for an unbiased sample of clusters.

In this Section we summarize the statistical and systematic errors associated with the SZ and X-ray observations, following the discussions in reports of the latest interferometric observations (from BIMA, Reese et al. 2000; and from the Ryle Telescope [RT], Grainge et al. 1999), and in review articles (Birkinshaw 1999). We also use some additional references to compile a detailed list of error sources.

3.1. Errors from measurements

Statistical errors from measurements in the angular diameter distance are dominated by counting statistics in X-ray images and spectra, and by Gaussian measurement uncertainties in the SZ measurements. These statistical errors propagate to errors in θ_c and β through fitting for the spatial distribution, and to errors in T_e , Λ_e , Z_{ab} , and N_H through fitting the X-ray spectrum. A simultaneous fit of a β model on interferometric SZ and X-ray images determines θ_c , β , S_{X0} and ΔT_0 (e.g. Reese et al. 2000), but causes the errors in these parameters to be strongly correlated.

The most important error sources in a determination of the angular diameter distance are the error in S_{X0} and the error in T_e (Eq. 5). The electron temperature enters the estimate of D_A roughly as T_e^{-2} , since for most X-ray observations to date the X-ray emissivity, $\Lambda_e(T_e, Z_{ab})$ is a slowly-varying function of T_e . Other uncertainties, from the dependence of Λ_e on the abundance of metals in the ICM and the absorbing column on the line of sight, are less important, and we can also neglect the contribution to the error in the angular diameter distance from the redshift.

The error in the spatial fit is dominated by the uncertainty in the central SZ decrement, ΔT_0 , and central X-ray surface brightness, S_{X0} . Both errors are about 8-10% in the data obtained using BIMA and ROSAT. The total uncertainty in a D_A estimate from spatial fitting to X-ray imaging and SZ interferometric measurements (with BIMA or the RT) is about 14-18%. We can expect a dramatic improvement in the accuracy of S_{X0} in the near future because of the larger collecting area and higher angular resolution of XMM and Chandra, and because the improved imaging will also allow a better choice of models for the ICM. A substantial improvement in the central SZ effect is also likely, as the first generation of dedicated SZ interferometers becomes available. The overall statistical error in these parameters should drop to about 4-5%.

The statistical errors in measurements of electron temperature based on ASCA and ROSAT observations are up to about 15-20% (Reese et al. 2000; Grainge et al. 1999). With today’s technology (Chandra and XMM), a 5% statistical error in the emission-weighted average electron temperature of a well-defined region of a high redshift cluster should be straightforward (David et al. 2001; Arnaud et al. 2001; Peterson et al. 2001).

The principal identified systematic errors in the measurements arise from the absolute calibration of the radio and X-ray observations. Errors in the effective area of the ROSAT PSPC and HRI introduce an error of about 10% in D_A . This error is greatly reduced (to 1-2%) for the instruments on Chandra and XMM-Newton. The absolute calibration error of radio interferometers is good to 4-5%, but could be improved to about 1% through extensive observations of point sources, tied to the planetary flux density/brightness temperature scale (Birkinshaw 1999).

Ground-based interferometric observations are also subject to systematic errors due to the removal of background (and cluster) radio sources, which may be imperfect if the sources are variable or have significant angular extent. Imperfect calibration of the phase and amplitude of the detector system may also cause errors near brighter contaminating sources. Fortunately interferometers are insensitive to large scale gradients in emission from the ground and atmosphere, and so this source of systematic offset signals from single-dish data is largely removed in interferometric work (e.g., Carlstrom et al. 2001).

3.2. Errors from modeling

The modeling of the structure of the ICM is an important part of determining the distance to a cluster, since it is the model that makes it possible to connect the LOS size of a cluster to its apparent angular size projected on the plane of the sky. Following most treatments in the literature, we use isothermal spherical β models to describe the IC gas distribution, and in this Section discuss the errors introduced by deviations from this model. As before, we can identify random and non-random systematic modeling errors.

Significant random modeling errors arise from the *asphericity* of the intra-cluster gas, the *peculiar velocity* of the cluster, and *primordial CMB fluctuations*. Serious non-random modeling errors can be expected from *non-isothermality*, *cooling flows*, *clumping*, *merging*, and *finite extent* of the cluster. Other issues that may be important are *radio point sources* and *gravitational lensing*. We briefly discuss random modeling errors from resolved radio halos in clusters because of their contribution to the measured SZ signal (through synchrotron emission) and to the X-ray signal (through inverse Compton emission), the effect of diffuse free-free emission from cool gas (for example in spiral galaxies), and finite optical depth effects.

3.2.1. Random modeling errors

Asphericity is one of the most important source of systematic errors in the determination of the distance to clusters when using a spherically symmetric isothermal β model. If the cluster is not spherical, the assumption that $r_c^{FIT} = r_c^{LOS}$ is invalid. We estimate the extent of this problem by approximating the true structures of clusters as oblate or prolate ellipsoids (or, more generally, as triaxial ellipsoids), while retaining the assumption that the distribution is described by an isothermal β model with constant β . If the symmetry axis is in the LOS, we would assume $r_c^{FIT} = r_c^{LOS}$, and thus overestimate (underestimate) D_A for prolate (oblate) clusters. Birkinshaw (1999) finds that prolate or oblate clusters with symmetry axis aligned in the LOS, if assumed spherical, will have a fractional error of

$$\frac{\delta D_A}{D_A} = \frac{a - b}{b}, \quad (6)$$

where $a (= r_c^{LOS})$ is the core radius in the LOS and $b (= r_c^{FIT})$ is the core radius in the plane of the sky ($a > b$ for a prolate distribution). Clusters often show ellipticity at the level, in projection, of $a/b = 1.25$ (Mohr et al. 1995). If the axis of symmetry is not in the LOS, the error is smaller, therefore the fractional error in D_A should be $< 25\%$. Hughes & Birkinshaw (1998)'s analysis of CL0016+16 showed that oblate or prolate distributions may cause less than 8% error in D_A if the structure of the ICM is analyzed as spherical. Grainge et al. (1999)'s work implies about a 14% error in D_A for Abell 1413.

N-body simulations can be used to understand the details of physics of the cluster geometry, and quantify the deviations from the spherical distribution. Inagaki et al. (1995)'s numerical simulations show that asphericity causes an error of up to 15% in D_A . Cluster merging simulations of Roettiger et al. (1997) show that small off axis merging in general causes prolate distributions, while oblate distributions may be caused by large off axis merging, causing typically less than 20% error in D_A . Observationally, Basilakos et al. (2000) found that prolate spheroid models fit the APM cluster data better than oblate spheroids. Sulkanen (1999) studied a statistical sample of clusters assuming a triaxial beta model density distribution. Sulkanen's results indicate that the distance scale obtained assuming a spherical distribution is within 14% of its true value (at 99.7% confidence) based on a sample of 25 clusters with triaxial axes consistent with observations (cf. also Puy et al. 2000).

In general, oblate or prolate clusters will have their axis randomly distributed in the sky. Zaroubi et al. (1998) studied general de-projections assuming that clusters have axially-symmetric density distributions with an arbitrary orientation of the symmetry axis. They found that using SZ and X-ray images one can determine only a combination of distance and inclination angle. Another image (weak lensing for example) is necessary to decouple these two parameters and determine the distance separately. If only X-ray and SZ data are available, the error that asphericity introduces into the D_A determination for any single cluster cannot be reduced below about 15%. However, the combination of X-ray, SZ and weak lensing data together with modeling of the equilibrium of the hot gas, should allow us to reduce the error to around 5%. The

planned weak lensing surveys should make the required lensing data available in the near future. Alternatively, galaxy velocity distributions from optical observations can be used with numerical simulations to determine physical parameters of individual clusters, as was done by Gomez et al. (2000) and Roettiger et al. (1997) (see the discussion of merging, below).

Peculiar velocities of clusters introduce enhanced (approaching) or decreased (receding cluster) SZ measurements because of the kinematic SZ effect (Sunyaev & Zel'dovich 1980; for a derivation cf. Birkinshaw 1999). In CDM models, cluster peculiar velocities are 400-500 km s^{-1} (Colberg et al. 2000; Ueda et al. 1993). This would introduce only a few percent error in D_A . However, some observations suggest larger peculiar velocities, 1000 km s^{-1} (Bahcall & Soneira 1983; Lauer & Postman 1994). If these large velocities are real, the kinematic SZ effect may cause an error of up to 25% in D_A . Fortunately one can separate the static and kinematic SZ effects based on their different frequency dependence or, equivalently, the peculiar velocities can be determined by measuring the cross-over frequency of the total SZ effect (e.g., Molnar & Birkinshaw 1999). Peculiar velocities also introduce a small bias in the redshift determination of the cluster. If clusters are selected based on their SZ signal, this effect would cause a biased sample of clusters, and a systematic overestimate of D_A would result.

Primordial CMB fluctuations introduce systematic effects in the distance determinations with their positive or negative contributions to the microwave decrement misinterpreted as SZ signal. The amplitude of systematic errors introduced by CMB fluctuations is a strong function of the observation strategy. The CMB fluctuations are reduced at arcminute angular scales compared to their degree-scale amplitudes, but still introduce a scatter of about 10% in the distance determinations (Cen 1998). At smaller scales (high ℓ s) the power in CMB fluctuations becomes negligible. A further reduction in the level of this error can be achieved using spectral separation of the thermal SZ effect from the primordial fluctuations (and the kinematic SZ effect). Gravitational lensing transfers power from large scale primordial fluctuations to small scale fluctuations (Metcalf & Silk 1998; Seljak 1996). As a result, if the CMB is not separated from the SZ effect, it would give larger, but a symmetric scatter in D_A , or a fractional error of about 8% (Cen 1998). Note, however, that the kinematic SZ effect and primordial CMB fluctuations have the same frequency dependence, thus they can not be separated from each other based on their frequency signature. Fortunately both effects can be separated out from the static SZ effect simultaneously, based on their different frequency dependence.

The errors in the cosmological parameters caused by random modeling errors (asphericity, cluster peculiar velocities, and primordial fluctuations, etc...) can be reduced using a properly-selected sample of clusters. This sample must avoid selection biases that themselves introduce systematic errors. As was emphasized by (Birkinshaw et al. 1991), clusters should not be selected based on their SZ or X-ray central brightnesses, since such a selection would produce a sample containing an excess of clusters with prolate geometry, high positive peculiar velocity in the LOS,

and contamination from negative CMB fluctuations (if the Rayleigh-Jeans frequency band is used), and result in a biased D_A . X-ray selected clusters with a flux limit well above the detection limit might be used as in Mason et al. (2001) and Jones et al. (2001). Alternatively, if there are multi-frequency measurements, the best solution would be to separate the kinematic SZ effect and the primordial fluctuations from the static SZ effect, and use the total static SZ effect flux density as a selection criterion.

3.2.2. Non-random modeling errors

Non-isothermality is one of the major sources of systematic error in the determination of D_A .

The isothermal assumption for the intra-cluster gas is clearly an approximation. Even if the central region of cluster is virialized and isothermal, the outer regions will be subject to shocks from merging and gas in-falling from filaments. Merging with massive clusters will change the temperature relative to the single-component cluster virialized value, even in the core region. Observations show that the central regions are nearly isothermal, but thermal substructures have also been found in clusters (Sarazin 1988). The effect of temperature variations on the distance estimate depends on the instrumentation and observing technique used. SZ measurements are insensitive to temperature variations in the cluster if the projected pressure profile is unchanged. Non-spatially resolved X-ray measurements determine emission weighted temperatures, and so are sensitive to the thermal structure of the central region of clusters. Thus the temperature deduced from X-ray measurements is well suited to comparison with SZ measurements by radio interferometers, which also most sensitive to the central region and have less response to the outer parts of the cluster (for example, assuming 2σ detection, BIMA is sensitive out to about $3r_c$, and about 85% of the observable X-ray flux of a typical cluster, using ROSAT PSPC, is within $3r_c$).

Birkinshaw & Hughes (1994) and Holzapfel et al. (1997) analyzed Abell 2218 and Abell 2163 respectively, assuming an isothermal β model and a model with falling temperature with radius. Their results show that D_A may be overestimated by 20-30% if non-isothermal distributions are assumed to be isothermal. Numerical simulations show similar errors due to non-isothermality: thus Inagaki et al. (1995)'s simulations lead us to conclude that an overestimate of 25% in D_A , mostly because of the overestimated SZ amplitude, may result from assuming isothermality when the temperature is lower in the outer regions. Simulations of merging clusters by Roettiger et al. (1997) obtained a similar result, that an overestimate of 10-30% may result in D_A from non-isothermality, with the range depending on the projection geometry. Note, however, that these results are based on single-dish measurements: for interferometric observations these effects are usually smaller.

It is not easy to correct for non-isothermality. The SZ effect is proportional to $\langle n_e T_e \rangle R_{char}^{LOS}$, and for an accurate calculation of the SZ effect, it is often necessary to have good information about the temperature out to R_{vir} (about $10r_c$) or more. It is difficult to carry out spatially resolved spectroscopy at such large radii because of the low X-ray surface brightness of the outer regions of clusters

($S_X \propto n_e^2$). At present, the best evidence from BeppoSAX data extends $T(r)$ measurements to $(0.5 - 0.75)R_{vir}$ (Irwin & Bregman 2000; De Grandi & Molendi 1999). The increased sensitivity available with Chandra and XMM should enable us to use spatially resolved spectroscopy to determine the temperature profiles of clusters which both resolve the inner cooling flow region and collect enough photons to measure useful temperatures in the clusters' outer regions (Schmidt, Allen & Fabian 2001; Tamura et al. 2001).

Unfortunately the hydrostatic equilibrium assumption of the β model breaks down in the central parts of clusters with high enough density for cooling to be important. In these cases the ICM will radiate via thermal bremsstrahlung and line emission (with the balance depending on the temperature), and develop a pressure gradient and a sub-sonic inflow, a so-called *cooling flow* (see review of Fabian 1994). The increased central density at the core of the cluster leads to an increased level of X-ray emission, which is often used as an indicator of the presence of a cooling flow region.

Phenomenological models have been developed and numerical simulations have been performed to study cooling flows (White & Sarazin 1987; Rizza et al. 2000; Fabian 1994, and references therein). Majumdar and Nath (2000) estimated the effect of cooling flows on the determination of the Hubble constant. They found that only at the very center of the cooling flow (within the sonic radius) will the X-ray luminosity drop because of the decreased temperature of the ICM. They show, further, that there is a gradual increase in pressure towards the center of the cooling flow. Outside this region, the approximation of hydrostatic equilibrium profile remains good, while within there will be an SZ effect excess. Thus Majumdar & Nath (2000)'s results indicate that one should exclude 80% of the cooling flow region to reduce the error in D_A to below 10%. However, this may be an upper limit on the error in D_A , since the calculation ignored the effect of the cooling flow on the structure fitting. Fig. 3 and 4 in Reese et al (2000) suggest that a compensatory error occurs here, and this lowers the error in D_A .

A further effect from cooling flows, pointed out by Schlickeiser (1991), is that the build-up of cold gas at the center of cooling flows might lead to significant free-free emission in the radio band, which would reduce the SZ signal. This works in the opposite sense to the pressure effect, but provides another reason for excluding the central parts of SZ images of cooling flow clusters from the SZ/X distance scale analysis.

Excluding cooling flow clusters completely from SZ/X distance scale studies would be the most complete solution to the problem that they pose. However, most clusters close to hydrostatic equilibrium (where the underlying physics required to model the ICM is most straightforward) possess cooling flows. Modeling cooling flows, and excluding their centers, is therefore necessary to build up large samples for Hubble constant work.

High-redshift cooling flow clusters can be recognized by using their X-ray spectra even if we cannot resolve the central region, since cooling flow clusters have emission weighted metallicity 1.8 times higher than non-cooling flow clusters (Allen & Fabian 1998). Mohr, Mathiesen &

Evrard (1999) analyzed nearby cluster of galaxies using ROSAT PSPC data, modeling cooling flow regions where necessary, and found that fitting an isothermal β model to cooling flow clusters will underestimate both r_c and β , and therefore produce a poor fit even outside the cooling flow. They identified cooling flow clusters based on two criteria: 1, non-random residuals consistent with a central emission excess; and 2, relaxed cluster with no asphericity or sub-structure. They concluded that a double β model fit gives an unbiased estimate of D_A . Cooling flow contamination in the determination of the average Hubble constant using the SZ/X ray method can be recognized by searching for a dependence of individual Hubble constants (determined for each cluster) on IC gas metallicity.

Clumping in the IC gas is potentially one of the most important systematic effects. It is well known that radio halos, hot bubbles from supernova eruptions, cold condensed gas in galaxies, etc. constitute a level of clumpiness in the ICM. The important question is whether the effect of clumping is important in the SZ/X method of measuring D_A .

As a first approximation, clumping will enhance the X-ray surface brightness since $S_X \propto n_e^2$, and does not change ΔT_{SZ} , since ΔT_{SZ} is proportional to the line-of-sight averaged pressure and clumps should be in pressure equilibrium with their surroundings if they are to be long-lived (assuming no substantial magnetic fields exist). As a consequence, D_A is underestimated. However, the emission-weighted temperature of the cluster measured by X-ray spectroscopy will also decrease. This reduces the systematic effects of clumping to only a few percent error in D_A . Birkinshaw, Hughes & Arnaud (1991) studied the effects of isobaric clumping of the intra-cluster gas in Abell 665. The fractional error in D_A from clumping is

$$\frac{\delta D_A}{D_A} = \frac{\langle n_e \rangle^2 < \Lambda(T_e) \rangle}{\langle n_e^2 \Lambda(T_e) \rangle} - 1, \quad (7)$$

where the angle brackets imply averages over regions larger than the scale of the clumping. For isothermal clumps Λ_e factors out. Then since $\langle n_e^2 \rangle / \langle n_e \rangle^2$ is always greater or equal to 1, clumping will always cause an underestimate of D_A . Birkinshaw et al. (1991) found $\langle n_e^2 \rangle^2 / \langle n_e \rangle^2 < 3$ or so. Holzzapfel et al. (1997) studied the effects of isobaric clumping on Abell 2163. Assuming cold clumps they estimate that error from clumping could lead to an overestimate of about 10% in D_A .

Inagaki et al. (1995) find, from their $\Omega_m = 1$ numerical simulations, that D_A will be underestimated by about 15% due to clumping. However there is evidence that lower matter density models produce less clumpy structures, so that if our Universe has $\Omega_m < 1$, Inagaki et al. will have overestimated the effect of clumping.

Self-consistent modeling of small scale clumping is difficult because many physical processes contribute to its creation and destruction. Gunn & Thomas (1996) used phenomenological multi-phase models to study X-ray emission from clumpy IC gas. Their isobaric model implies a fractional error in the X-ray central surface brightness

$$\frac{\delta S_X(0)}{S_{x0}} \propto \frac{\langle n_e \rangle \langle n_e^{1-\alpha} \rangle^{\alpha/2}}{\langle n_e^{-\alpha} \rangle^{(1+\alpha)/2}}, \quad (8)$$

where α is the emissivity exponent. This would cause about a 10% error in D_A .

Nagai et al. (2000) discussed biases in the Hubble constant determination from a multi-phase, spherically-symmetric, intra-cluster medium with isobaric clumping of variance

$$\sigma^2 = \frac{\sigma_c^2}{(1 + (r/r_c)^2)^\epsilon}, \quad (9)$$

where σ_c and ϵ are free parameters describing the strength and radial dependence of the variance. They assumed a log-normal distribution for the gas density phase distribution, which was motivated by simplicity and the effect of non-linear gravitational growth of initially Gaussian density fluctuations (Cole, Fisher and Weinberg 1994). They assumed that the multi-phase model has the same emission weighted temperature and the X-ray emission profile as a fiducial single phase model. Based on their results, the error in the distance from an incorrect assumption of a single-phase ICM is

$$\frac{\delta D_A}{D_A} = 2 \exp\left[\frac{(1-\alpha)(2-\alpha)}{4} \sigma_c^2\right] - 1, \quad (10)$$

where α is again the power-law exponent in the emissivity function. We can conclude that clumping may cause a 5 – 20% error in D_A .

Spatially-resolved X-ray spectroscopy, as can be performed using Chandra and XMM, will help to estimate the clumpiness of the IC gas. Emission lines between 0.5 and 1.5 keV originating in cool regions, such as the Fe L-shell lines, H- and He-like lines from N, O, Ne, Mg, will provide a strong test on multi-phase models. Unfortunately this method will not constrain all types of clumpiness. Hughes & Birkinshaw (1998), and Mason (1999) suggest that, since SZ/X Hubble constant determinations are not very different from the results of other methods, clumping introduces less than a 10% error. However, it is possible that clumping itself introduces more bias, but that this bias is balanced by other effects with opposing biases.

Roettiger et al. (1997) studied systematic errors in the Hubble constant from cluster *merging*. Merging can lead to the formation of shocks that compress and heat the IC gas. After a merger, the gas will settle into the prolate or oblate potential well defined by the dark matter distribution. As already discussed, ellipticity introduces scatter rather than bias in D_A . However, shock-heated IC gas will have different SZ and X-ray properties than gas in hydrostatic equilibrium, and its presence will introduce bias. Based on simulated X-ray images and temperature maps, Roettiger et al. find that isothermal assumptions in merging clusters systematically overestimate D_A by about 15%. Numerical simulations show that density enhancements due to merging of sub-clusters can result in higher X-ray surface brightness, change mass estimates, and might, if not recognized, cause an about 20% error in distance determination (Mohr et al. 1999).

Roettiger et al. (1997) suggest that clusters at the early stages of merging should be excluded from distance determinations. Dynamically active clusters may be recognized from their galaxy velocity distributions. Clusters with dynamical activity will have a large β discrepancy ($\beta_{fit} \neq \beta_{spect}$, see details in Sarazin 1988). Anisotropy in galaxy velocity distribution also signals dynamical activity. More relaxed systems, like merging clusters after they reached quasi-equilibrium may be modeled and included in

the distance determination. Simulations help to analyze individual merging clusters (Roettiger et al. 1995; Gomez et al. 2000): adjustments to the initial parameters of merging clusters are made until the resulting merged cluster has the observed SZ and X-ray appearance and galaxy velocity distribution.

The β model gives divergent masses if not truncated at some finite radius, which is usually taken to be about 10 core radii. This fact is a sign that at large radii, the beta model can not be correct. When calculating the distance to a cluster using the isothermal β model, we assume an infinite extent, and therefore the *finite extent* of clusters introduces a systematic bias in D_A . The SZ effect is more sensitive to outer regions than X-ray bremsstrahlung, since it is proportional to n_e unlike X-ray bremsstrahlung, which is prop to n_e^2 . In theory, the SZ effect measurements are more suitable for studying the outer regions of clusters, and also are subject of more error caused by the finite extent of clusters.

Inagaki et al. (1995) discussed the effect of finite cluster sizes. They find that the ratio between finite truncated and full beta models is

$$\frac{\delta D_A}{D_A} = \left[\frac{1 - \frac{B_q(3\beta/2 - 1/2, 1/2)}{B(3\beta/2 - 1/2, 1/2)}}{1 - \frac{B_q(3\beta - 1/2, 1/2)}{B(3\beta - 1/2, 1/2)}} \right]^2, \quad (11)$$

where $q = 1/(1 + p^2)$, $p = R_{cut}/r_{core}$, B and B_q are the beta and incomplete beta functions, and assuming no change in θ_c^{FIT} . Inagaki et al. (1995)'s results suggest that this effect can cause an about 10-20% underestimation of D_A for typical parameter values (cf. also Puy et al. 2000). By contrast, Birkinshaw & Hughes (1994) and Holzapfel et al. (1997), analyzing Abell 2218 and Abell 2163 respectively, find that finite cluster extent contributes only about 6% and 2% overestimate error in D_A . Observationally, Molnar (2000) attempted to find the outer cut off of Abell 3571 using RXTE scans across the cluster. Abell 3571 seems to extend well beyond its virial radius, however, this conclusion is not strong due to poor statistics in the data.

Clearly, more observations are needed to find out the extent to which the β model is correct, and how the transition happens from the cluster to the surrounding regions (dominated by filaments according to numerical simulations). A falling temperature profile with radius is a sign of deviations from the β model, and may provide the best tracer of additional structure of this type. We expect errors from this effect to be reduced greatly when the new spectral information from Chandra and XMM is available.

One of the most important contaminants of the SZ effect is emission from *radio point sources*. Such emission, especially at the center of the cluster, will decrease the fitted amplitude of the SZ decrement in the Rayleigh-Jeans frequency region, and cause an underestimate in the distance of the cluster. Using the sensitivity of the instrument, one can estimate the maximum flux density of unresolved point sources that can contribute to this error: for BIMA and the RT, the systematic errors are in the 10-15% range. The level of radio source confusion varies with the observing technique used. Multi-baseline interferometric observations have the most favorable confusion level. A deep survey, carried out at different frequencies or interferometer baselines, would help to find point sources up

to a limit when the error due to unresolved point sources would be negligible relative to other errors. Interferometric measurements also have the advantage over single-dish observations of being able to monitor the brightnesses of (potentially-variable) point sources while simultaneously measuring the SZ effect.

As Loeb & Refregier (1997) pointed out, systematic effects in the determination of the baseline for the SZ effect arise from *gravitational lensing* by the cluster gravitational potential. The brightnesses of point sources are enhanced by lensing, which brings them above the detection threshold, and thus they are removed from the field. This over-removal of point sources from the background lowers the background flux relative to a control field, and thus leads to an overestimate of the SZ signal, and an underestimate of about 10% of D_A . However, this effect is important only at frequencies less than about 30 GHz, and its presence can be tested (and corrected for) using the model cluster mass distribution which can be obtained by conventional analyses of the X-ray data for each cluster (cf. also Blain 1998).

Other, probably small, effects contributing to the error budget, which should be checked and treated individually when necessary are: contributions in the radio band from synchrotron emission from resolved halo (and other) sources in clusters, free-free emission from cool gas in spirals, free-free emission from radio halos in the X-ray band (Birkinshaw 1979), and any contribution from the non-thermal SZ effect. As was pointed out by Molnar & Birkinshaw (1999), the Kompaneets equation and its relativistic extensions are equivalent to a single scattering approximation, thus a small effect will arise from ignoring finite optical depth (multiple scattering). Any non-thermal population of IC electrons would produce a non-thermal SZ effect. There are some theoretical arguments for such a population (Petrosian 2001; Blasi 2000; Colafrancesco 1999; Sarazin 1999), and some observations have detected the expected excess hard X-ray emission (e.g., in the Coma cluster), but such excess X-ray emission is rare and hence the non-thermal electron population is weak (Fusco-Femiano et al. 2001; Maloney & Bland-Hawthorn 2001). Clusters with complex morphology should not be used for distance determinations because of the difficulty in their modeling. If substructure in high redshift clusters (as in RX J1347-1145, cf. Komatsu et al. 2001) is common, one should check such individual clusters for complex morphology using a high resolution instrument.

The *cumulative* systematic effect resulting from all these sources of error is best addressed via numerical simulations. Yoshikawa et al. (1998) used numerical simulations to estimate the systematic error from fitting β models to clusters. They used a spatially flat fiducial model with $\Omega_m = 0.3$, $\Omega_\Lambda = 0.7$, and $h = 0.7$ for their simulations. They found that the isothermal β model describes clusters well both in SZ and X-ray imaging. They found that, even though the fitted β model parameters were different when fitted to SZ or X-ray images (due to non-isothermality, non-asphericity, and clumpiness), the systematic errors in the Hubble constant (and so in distances) are negligible at low redshifts. At high redshift ($z \sim 1$), about a 20% overestimate of D_A might occur, mainly due to

non-isothermality and asphericity. Inagaki et al. (1995) find that the cumulative effect of non-isothermality and asphericity leads to about a 10 – 20% overestimate of D_A , since the overestimate due to non-isothermality is larger than the underestimate due to clumpiness (though in their simulations $\Omega_m = 1$).

3.3. Summary of the error budget

The new generation of satellites will allow us to determine more precisely the temperature profile and spatial structure of the intra-cluster medium, and thus minimize the systematic errors in D_A that result from temperature variations. When necessary, the spatial resolution of these new instruments will allow us to model the gas in each individual cluster beyond the spherical isothermal beta model. Numerical modeling of individual clusters will help us to derive their physical parameters. The improved spatial resolution will also allow us to study clumpiness, which is another important source of uncertainty. In general, those effects which have different spectral signature from the static SZ effect, should be separated from the SZ effect using multi-frequency observations.

Based on our evaluation of the error budget, we estimate that the random error in D_A achievable in the near future using known techniques, and assuming that lensing measurements will be used to eliminate errors from cluster asphericity, might be as low as 7%. This estimate is made up by quadrature combination of the errors, with the dominant terms being from T_e (5%) and spatial fitting (5%). A systematic error of 5% might also be obtained, although this would be difficult.

Evolution effects are clearly important limitations in determining cosmological parameters. The advantage of the SZ/X-ray method is that, as long as hydrostatic equilibrium and simple geometry hold, it should be reliable even if scaling laws (for example mass - temperature) evolve. However, a detailed analysis of evolution effects is out of the scope of our paper. We restrict ourselves to simply studying the effect of an additional systematic error in the D_A determination with a linear gradient with redshift.

4. CONSTRAINTS ON COSMOLOGICAL PARAMETERS

As discussed earlier, in the near future SZ surveys will discover hundreds of high and low redshift clusters, and we can expect Chandra and XMM observations of hundreds of clusters. However, accurate angular diameter measurements require long SZ and X-ray integrations and therefore we do not expect all discovered clusters to have accurate SZ/X distance measurements. If the SZ/X method is to be used to measure cosmological parameters, we should select a sample of clusters that minimize the systematic errors (Section 3) while not requiring excessive observing time. As pointed out in Huterer & Turner (2000), the ideal distribution of clusters in redshift space would be a superposition of P delta functions in redshift, where P is the number of cosmological parameters to be determined. In practice, however, in any narrow redshift band we will not have enough clusters to achieve good statistics, and objects at $z > 1$ would need excessive integration times to reach high individual accuracies. A detailed study to select the optimum redshift distribution of clusters, taking into account the differing numbers of suitable clusters at

different redshifts and the detailed characteristics of the possible instruments and observational strategies is beyond the scope of our paper and more properly devolves on the groups proposing to construct such instruments. Here we do a simpler problem, by assuming that distances with similar accuracies are available for a set of clusters uniformly distributed in redshift space between $z = 0.01$ and $z = 1$. This choice covers almost half of the redshift interval most sensitive to the cosmological constant ($z = 0.5 - 1.8$), but excludes the more distant objects for which excessive integration times would be needed.

We carried out simulations to estimate the constraints from the angular diameter distance-redshift function on the parameter space defined by Ω_m , Ω_Λ , and h , and also by Ω_m , w , and h (assuming a spatially flat geometry $\Omega_\Lambda = 1 - \Omega_m$). We simulated clusters using a spatially flat fiducial CDM model with $\Omega_m = 0.3$, $\Omega_\Lambda = 0.7$, and $h = 0.65$. We use the χ^2 statistic to evaluate errors from our simulations, since we are dealing with large errors, 50% in cosmological parameters, and therefore the assumptions leading to the Fisher matrix formalism are not satisfied. We choose realizations which have best fit values close to those of the input fiducial model, and offset by the values of $\Delta\chi^2 = 3.53$, 8.02 and 14.2 appropriate for the number of fitted parameters to find the Gaussian 1, 2, and 3 σ error surfaces (defined by probability levels of 68%, 95.4%, and 99.73%).

As a first realization, we assumed a sample of 500 clusters uniformly distributed in redshift (so that 250 lie at $z > 0.5$) with 4% random error in D_A , which might be achieved if systematic errors can be tightly controlled (we assume lensing measurements will be used to eliminate errors from cluster shape). We use these results to demonstrate the ultimate constraints on cosmological parameters that might be achievable from the SZ/X-ray method. In Figures 2a, b, and c, we show the results of fitting cosmological parameters to the observationally-determined angular diameter distance function (1, 2, and 3 σ concentric ellipses, solid lines, assuming three independent parameters, corresponding to $\Delta\chi^2$ of 3.53, 8.02 and 14.2 appropriate for three fitted parameters). 2-dimensional (2D) projections of the 3D surface of 3 σ constraints are shown using dotted lines. In the $\Omega_m - \Omega_\Lambda$ plane (Figure 2a) the error ellipses are elongated roughly along the line $2\Omega_m - \Omega_\Lambda = \text{constant}$. This is similar to the constraint obtained from the SNe Ia experiment, which measures cosmological parameters via the predicted apparent magnitude distribution, and uses different redshift limits. Very low redshift measurements of clusters lead to error ellipses which are elongated along the line $\Omega_m - 2\Omega_\Lambda = \text{constant}$. As higher redshift objects are added, this elongated feature rotates counter-clockwise. From Figure 2c, which shows constraints in the $h - \Omega_\Lambda$ plane, we can conclude that with the assumed accuracy, the cosmological constant is not well constrained. However, h is well measured even without additional information. In general, the dispersion of measurements (1, 2, 3 σ contours) is determined by random and not systematic errors. Systematic errors introduce only bias, shifting the mean of the measurements away from the expected value in the parameter space while preserving their dispersion. A $\pm 3\%$ systematic error in the D_A will not affect the results in the $\Omega_m - \Omega_\Lambda$ plane, but

simply shift the error ellipses we obtained from random errors up or down along the h axis by 0.02 (3% of the fiducial value of h), since the amplitude of D_A is set by the Hubble constant (Figures 2ab and c, 3σ solid ellipses above and below the 1, 2, and 3σ concentric ellipses corresponding to random errors, solid lines). With the assumed random and systematic errors, the determination of h becomes limited by systematic errors. We also carried out simulations assuming a systematic error with a gradient in redshift growing from 0% at $z = 0$ to $\pm 3\%$ at $z = 1$ in addition to the assumed 4% random error to study the effect of evolution. (Figures 2b and c, short dashed and dash dotted 3σ lines). The error ellipses from random errors will be shifted in the $\Omega_m - \Omega_\Lambda$ plane (Figure 2a). From Figures 2b and c we can conclude that the Hubble constant will not be affected by this type of systematic errors, which follows from the fact that the Hubble constant is constrained by the low redshift regime where the assumed systematic errors are small. Ω_m and Ω_Λ are strongly affected since their relation is determined by redshift between 0.5 and 1.8 (cf. Figure 1), where the systematic errors become larger, thus Ω_m and Ω_Λ become limited by this type of systematic errors. An indication of systematic errors in D_A from evolution might be found using an $\Omega_m - h$ plot (Figure 2b).

In Figures 3a, b, and c we show similar constraints on Ω_m , w , and h from the SZ/X-ray method using the same fiducial CDM model, and 500 clusters with a random error of 4% in D_A , as before (1, 2, and 3σ concentric ellipses, solid lines). The constraints form a banana-shaped region elongated in the $\Omega_m - w$ plane (Figure 3a). Systematic errors in the D_A will not affect the results in the $\Omega_m - w$ plane, but simply shift the ellipses from random errors up or down along the h axis (Figures 3b and c, 3σ solid ellipses above and under the 1, 2, and 3σ concentric ellipses of random errors, solid lines). Again, with the assumed 4% random and $\pm 3\%$ systematic errors, the h determination is going to be limited by systematic errors. We also carried out simulations adding a systematic error with a gradient in redshift growing from 0% at $z = 0$ to $\pm 3\%$ at $z = 1$ to the assumed 4% random error (Figures 3b and c, short dashed and dash dotted 3σ lines). Again, we find that Ω_m , and w are strongly affected, their determination is limited by the assumed systematic errors. As before, the Hubble constant determination is not affected by this type of systematic errors. Also, an indication of systematic errors in D_A from evolution might be found using a $w - h$ plot (Figure 3c).

From Figure 2c, which shows constraints in the $\Omega_\Lambda - h$ plane, we can conclude that with the assumed accuracy, the cosmological constant is not well constrained. From Figure 3a we can see that w is also poorly constrained by the SZ/X method. Clearly, whichever set of parameters is to be estimated, other cosmological measurements are needed to constrain these parameters further.

One of the most promising other experiments to measure cosmological parameters is based on CMB fluctuations. We estimated how well we can determine cosmological parameters if we add constraints from CMB experiment, which we would expect to be particularly useful since the strongest dependency in this experiment is on the space curvature (the total average density in the

Universe). As an illustration of the power of combining these techniques, we used the position of the first Doppler peak in the angular power spectrum of CMB fluctuations (Hanany et al. 2000; Mauskopf et al. 2000; Miller et al. 1999), and the combination $\Omega_m h^2 = \text{constant}$ as observables from primordial fluctuation studies (see for example Zaldarriaga, Spergel & Seljak 1997).

The position of the first Doppler peak can be expressed as

$$\ell_{peak} = k_{peak} r(z_*), \quad (12)$$

where k_{peak} and $r(z_*)$ are the first peak in k space and the effective distance to the last scattering surface at z_*

$$r(z_*) = \frac{1}{\sqrt{K}} \mathcal{S} \left[\sqrt{K} (\eta(0) - \eta(z_*)) \right], \quad (13)$$

where K is the curvature, \mathcal{S} is the sin, sinh, and identity function for models with negative, positive and flat space-time, and η is the conformal time. In k -space in a CDM model,

$$k_{peak} \approx c_1 + c_2 w_m + c_3 w_m^2 + c_4 w_b + c_5 w_b^2 + c_6 w_m w_b, \quad (14)$$

where $w_m = \Omega_m h^2$ and $w_b = \Omega_b h^2$, and the coefficients are: $c_1 = 0.0112$, $c_2 = 0.0441$, $c_3 = -0.043$, $c_4 = -0.0496$, $c_5 = 2.65$, and $c_6 = 0.162$ (White 1998). We used Hu & Sugiyama (1996)'s approximation for the redshift of the last scattering surface

$$z_* = 1048 [1 + 0.0012 w_b^{-0.738}] [1 + g_1^2], \quad (15)$$

where

$$g_1 = \frac{0.0783 w_m^{-0.238}}{1 + 39.5 w_m^{0.763}}, \quad (16)$$

and

$$g_2 = \frac{0.560}{1 + 21.1 w_b^{1.81}}, \quad (17)$$

In Figures 2a, b and c we over-plot the 3σ error region based on the position of the first Doppler peak in the CMB power spectrum (long dashed lines). This region is roughly aligned along the line $\Omega_m + \Omega_\Lambda = \text{constant}$ because of the strong dependence of the position of the first Doppler peak on the total space curvature. For demonstration purposes, we choose $\ell_{peak} = 245 \pm 10$, where we assume a 3σ error range of $\Delta\ell = 10$. As expected, constraints on cosmological parameters from SZ/X distance-redshift relation and the position of the first peak in the CMB fluctuations are highly complementary. For our assumed set of clusters, uniformly sampled in $z < 1$, these two constraints are nearly orthogonal to each other in the $\Omega_m - \Omega_\Lambda$ plane (Figure 2a). The constraints are also complementary in the $h - \Omega_m$ and $h - \Omega_\Lambda$ planes (Figures 2b and c). Geometrically, we have narrow banana-shaped constraints from the SZ/X-ray method elongated in the $\Omega_m - \Omega_\Lambda$ plane and narrow sheet-like constraints $h = \text{constant}$ from the position of the first peak of the CMB fluctuation spectrum. The intercept of these constraints gives us stringent constraints on the following cosmological parameters: Ω_m , Ω_Λ , and h can be determined to ± 0.08 , ± 0.1 , and ± 0.015 (3σ , assuming 4% random error in D_A). Note, that while the effect on Ω_m and Ω_Λ from reasonable redshift independent systematic errors are negligible, h would be dominated by systematic errors: a $\pm 3\%$ systematic error would result a ± 0.02 change in h . A systematic error which grows from 0% to $\pm 3\%$ at $z = 1$ would cause an additional ± 0.05 ,

± 0.05 , and ± 0.005 error in Ω_m and Ω_Λ , and h . Constraints from the SZ/X-ray method are also orthogonal to those from cluster evolution (compare constraints on the $\Omega_m - \Omega_\Lambda$ plane, our Figure 2a and Figure 1 of Holder et al. 2001). In Figures 2a, b and c we also over-plot constraints from $\Omega_m h^2 = \text{constant}$ assuming a 10% error in its determination from CMB experiments (dash dot dot dotted lines), as suggested by studies based on the characteristics of the MAP experiment (Zaldarriaga et al. 1997). These constraints seem to be less useful in this parameter space than those from the position of the first Doppler peak.

Constraints from the location of the first peak in the CMB fluctuations are not so useful when considering the alternative set of parameters w , Ω_m , h . The $\ell \approx 210 - 240$ constraint leads to surfaces which lie almost parallel to the ellipsoids derived from the SZ/X-ray method (compare our Figure 3a and Figure 4 of White 1998). In Figures 3a, b, and c we over-plot constraints from $\Omega_m h^2 = \text{constant}$ again assuming a 10% error in its determination (dash dot dot dotted lines). Combining constraints from the SZ/X-ray method and those from $\Omega_m h^2 = \text{constant}$ (based on CMB fluctuation analysis), we obtain stringent constraints on w and h (≤ 0.2 and ± 0.015 , 3σ). Note, that the effect on w from redshift independent systematic errors is negligible, and that, as before, h is dominated by systematic errors: a $\pm 3\%$ systematic error would result a ± 0.02 change in h . A systematic error which grows from 0% to $\pm 3\%$ at $z = 1$ would cause an additional ± 0.1 in w . From Figure 3b ($\Omega_m - h$ plane), we see that a gradient in the systematic error in redshift might be recognized using the $\Omega_m h^2 = \text{constant}$ constraint. Also, constraints from the shape of the power spectrum of CMB fluctuations (as will be achieved by MAP and Planck) are nearly orthogonal to those from the SZ/X-ray method (compare our Figure 3a and Figure 13 of Huterer and Turner 2000). Comparing our Figure 3a to Figures 8 and 9 of Haiman et al. (2000), we can see that constraints on the $\Omega_m - w$ plane from distance function and cluster evolution are complementary. Also, constraints on w from the SZ/X-ray method combined with cluster abundance would put stringent constraints on w .

Since the banana-shaped constraints from the SZ/X method in the parameter spaces defined by $(\Omega_m, \Omega_\Lambda, h)$ or (Ω_m, w, h) are nearly orthogonal to constraints from cluster evolution, a strategy for determining cosmological constants based *only* on clusters is likely to be successful. It seems to be possible to choose the parameters of the set of clusters used in this work such that constraints from the SZ/X ray method and cluster evolution can be made orthogonal, and thus optimized for separating cosmological parameters. Clusters can provide a powerful, independent test for cosmological parameters.

Note that our constraints in the $\Omega_m - w$ plane are curved towards the w axis (Figure 3a, solid and dotted lines), while Huterer & Turner (2000)'s constraints from SNe Ia (which is basically a constraints from distance - redshift function, cf. their Figure 23) show no sign of curvature. This is due to the fact that they used the Fisher matrix formalism, and we evaluated the χ^2 statistic directly. Our results show that the likelihood function is strongly non-Gaussian on the $\Omega_m - w$ plane.

As a second realization, we carried out simulations with

seventy clusters (35 high redshift clusters, $z > 0.5$), a number likely to be observed in the next few years, and estimated how well we can constrain cosmological parameters. We assumed the same fiducial cosmological model as before: $\Omega_m = 0.3$, $\Omega_\Lambda = 0.7$, and $h = 0.65$. For this simulation, however, we assumed a random error of 7% in the angular diameter distance, which might be achievable in the near future (we assume lensing measurements will be used to eliminate errors from cluster shape).

In Figures 4a, b, and c, we show the resulting 1, 2 and 3σ constraints on the parameter space defined by $(\Omega_m, \Omega_\Lambda, h)$, corresponding to $\Delta\chi^2$ of 3.53, 8.02 and 14.2 appropriate for three fitted parameters (solid lines). Long dashed lines show the constraints from the position of the first Doppler peak. As before, we assumed $\ell_{peak} = 245 \pm 10$ (3σ range). We also over-plot constraints from $\Omega_m h^2 = \text{constant}$ assuming a 10% error in its determination from CMB experiments (dash dot dot dotted lines). From these Figures we conclude that by using as few as 35 high-redshift (and 35 low-redshift) clusters, with a random error of 7% in D_A we can constrain Ω_m , Ω_Λ and h within ± 0.2 , ± 0.2 , and ± 0.04 (3σ errors). Note, that the effect of redshift independent systematic errors in D_A on Ω_m and Ω_Λ , occurring in practice, is negligible, but a $\pm 5\%$ systematic error would result an additional ± 0.035 error in h . Assuming that we know that our redshift independent systematic error is less than 15% at the 3σ level, with a 7% random error combined in quadrature, we would be able to determine h with an error of ± 0.11 . A systematic error which grows from 0% to $\pm 5\%$ at $z = 1$ would cause an additional ± 0.1 , ± 0.1 and ± 0.01 error in Ω_m , Ω_Λ , and h (Figure 4, short dashed and dash dotted lines). This means that as few as seventy clusters, with the errors likely to be achieved in the next few years, would be sufficient to exclude models with zero cosmological constant with high significance. These results would be independent of the SNe Ia data, thus they would provide a robust check to the supernova results.

In Figures 5a, b, and c, we show the 1, 2 and 3σ constraints on the parameter space defined by (Ω_m, w, h) , with the $\Omega_\Lambda = 1 - \Omega_m$ constraint (solid lines). We over-plot constraints from $\Omega_m h^2 = \text{constant}$ assuming a 10% error as before (dash dot dot dotted lines). From Figure 5a we can see that we will be able to determine the equation of state parameter, w , with accuracy of 0.45 (3σ), even with reasonable systematic errors in D_A , with additional information from CMB experiments, or SZ effect number counts. A systematic error which grows to $\pm 5\%$ at $z = 1$ would cause an additional error of 0.2 in w (Figure 5, short dashed and dash dotted lines).

5. CONCLUSION

We have estimated the accuracy achievable in the determination of cosmological parameters using the SZ/X-ray method of distance determination. This method uses a sample of clusters to map the distance-redshift relation, which is a sensitive probe of cosmological parameters. The advantages of this well-known method are: (1) unlike other distance determination methods, it depends only on the geometry of the Universe, and its average densities; (2) it is a physical method, based on relatively simple gravitational virialization of clusters (as opposed to complicated

physics and chemistry involved in galaxy formation and supernova explosions); and (3) a large number of clusters is available for observation, and thus systematic effects can be reduced by using many clusters, or selecting clusters appropriately to reduce systematics. The necessary data should be available within the next few years.

The SZ/X method, as other cosmological tests, can constrain well only some combination of cosmological parameters. We have shown that constraints on $(\Omega_m, \Omega_\Lambda, h)$ from the $D_A(z)$ function measured in $z = 0 - 1$ are nearly orthogonal to constraints from the first peak of the CMB fluctuations, and also to constraints from cluster evolution. Constraints on (Ω_m, w, h) from the $D_A(z)$ function are complementary to those from cluster evolution (compare our Figure 2 to Figures 8 and 9 from Haiman et al. 2000). In general, D_A provides constraints on cosmological parameters similar to those from the SNe Ia method. Constraints from cluster evolution (the source counts $N_{SZ}(z)$ and $N_X(z)$) are similar to constraints from the full CMB fluctuation spectrum as will be measured by MAP and Planck.

This result suggests that cosmological tests using *only* clusters of galaxies can be an important independent check on the values of cosmological parameters measured by other techniques. Cluster-based methods have systematic errors which are unrelated to those of other methods of measuring cosmological parameters (e.g., from CMB fluctuations, and SNe Ia). Furthermore, when the set of cosmological parameters is further extended, with additional components of density or structure parameters, joint analyses using multiple cosmological tests will be essential to remove the parameter degeneracy exhibited by any one test.

We demonstrated the effect of systematic errors on the determination of cosmological parameters. If random errors can be kept at a few percent level, systematic errors of similar magnitude will dominate the error in the Hubble

constant. Ω_m , Ω_Λ , and w are not affected by redshift-independent systematic errors. We also showed that a systematic error with a linear gradient in redshift will not affect Hubble constant determinations, but causes systematic shifts in the estimates of Ω_m , Ω_Λ , and w .

We showed, that in the near future, even with only 35 high redshift (and 35 low redshift) clusters, the SZ/X-ray method, combined with the position of the first peak in the power spectrum of CMB fluctuations, will provide enough accuracy to exclude $\Omega_\Lambda = 0$ models with high confidence even with constant and redshift dependent systematic errors (see Figure 4a). Also, the SZ/X-ray method, combined with the $\Omega_m h^2 = \text{constant}$ constraint, or cluster abundance, will allow us to determine the equation of state parameter, w , to within 0.45 (3σ ; Figure 5a), even with usual (redshift-independent) systematic errors.

This idealized discussion of the SZ/X-ray method and its errors in the determination of cosmological parameters could be improved by using the detailed characteristics of specific instruments and observing strategies. Departures from the assumptions made here could cause increases or decreases in the level of error in the derived parameters, with the largest changes likely for different redshift samplings.

We conclude, that the determination of the angular diameter distance - redshift function using the SZ effect and X-ray thermal bremsstrahlung emission from clusters of galaxies can be used with confidence to constrain cosmological parameters. In general, clusters of galaxies *alone* can be used to constrain cosmological parameters independently from other methods. Clusters lead to parameter limits which are competitive with using other techniques.

Most of this work was done while SMM held a National Research Council Research Associateship at NASA Goddard Space Flight Center. We thank David Spergel and the anonymous referee for useful comments and suggestions.

REFERENCES

- Arnaud, M., Neumann, D. M., Aghanim, N., Gastaud, R., Majerowicz, S., & Hughes, J. P., 2001, *A&A*, 365, L80
 Allen, S. W., & Fabian, A. C., 1998, *MNRAS*, 297, L63
 Balbi, A., et al. 2000, *astro-ph/0005124*
 Bahcall, N. A., & Soneira, R. M., 1983, *ApJ*, 270, 20
 Basilakos, S., Plionis, M., & Maddox, S. J., 2000, *astro-ph/0002459*
 Bartlett, J. G., 2000, *astro-ph/0001267*
 de Bernardis, P. et al., 2001, *astro-ph/0105296*
 Birkinshaw, M., 1979, *MNRAS*, 187, 847
 Birkinshaw, M., 1999, *Physics Reports*, 310, 97
 Birkinshaw, M., & Hughes, J. P., 1994, *ApJ*, 420, 33
 Birkinshaw, M., Hughes, J. P., & Arnoud, K. A., 1991, *ApJ*, 379, 466
 Blain, A. W., 1998, *MNRAS*, 297, 502
 Blasi, P., 2000, *astro-ph/0008113*
 Bridle, S. L., et al., 1999, *astro-ph/9903472*
 Browne, I.W.A. et al. 2000. *SPIE*, 4015, 299
 Carlstrom, J. E., et al., 2001, *astro-ph/0103480*
 Cavaliere, A., & Fusco-Femiano, R., 1976, *A&A*, 49, 137
 Cavaliere, A., Danese, L., & De Zotti G., 1979, *A&A*, 75, 322
 Cen, R., 1998, *ApJ*, 498, L99
 Challinor, A., & Lasenby, A., 1998, *ApJ*, 499, 1
 Colafrancesco, S., 1999, *astro-ph/9907329*
 Colberg, J. M., et al., 2000, *MNRAS*, 313, 229
 Cole, S., Fisher, K. B., & Weinberg, D. H., 1994, *MNRAS*, 267, 785
 David, L. P., et al., 2001, *astro-ph/0010224*
 De Grandi, S., & Molendi, S., 1999, *astro-ph/9911039*
 Diego, J. M., Martinez-Gonzales, E., Sanz, J. L., Benitez, N., & Silk, J., 2001, *astro-ph/0103512*
 Efstathiou, G., & Bond, J. R., 1999, *MNRAS*, 304, 75
 Efstathiou, G., Bridle, S. L., Lasenby, A. N., Hobson, M. P., & Ellis, R. S., 1999, *MNRAS*, 303, L47
 Evrard, A. E., Summers, F. J., & Davis, M., 1994, *ApJ*, 422, 11
 Fabian, A. C., 1994, *ARAA*, 32, 277
 R.Fusco-Femiano, R., D.Dal Fiume, D., M.Orlandini, M., G.Brunetti, G., L.Feretti, L., & G.Giovannini G., 2001, *astro-ph/0105049*
 Gawiser, E., & Silk, J., 1998, *Science*, 280, 1405
 Gomez, P. L., Hughes, J. P., & Birkinshaw, M., 2000, *astro-ph/0004263*
 Grainge, K. et al., 1999, *astro-ph/9904165*
 Guerra, E. J., Daly, R. A., & Wan, L. 2000, *astro-ph/0006454*
 Gunn, K. F., & Thomas, P. A., 1996, *MNRAS*, 281, 1133
 Haiman, Z., Mohr, J. J., & Holder, G. P., 2000, *astro-ph/0002336*
 Hanany, S., et al., 2000., *ApJ*, 545, L5
 Holder, G.P., Mohr, J.J., Carlstrom, J.E., Evrard, A.E., & Leitch, E.M., 2000, *ApJ*, 544, 629
 Holder, G. P., Haiman, Z., & Mohr, J. J., 2001, *astro-ph/0105396*
 Holzappel, W. L., et al. 1997, *ApJ*, 480, 449
 Hu, W., & Sugiyama, N., 1996, *ApJ*, 471, 542
 Hu, W., Fukugita, M., Zaldarriaga, M., & Tegmark, M., 2000, *astro-ph/0006436*
 Hughes, J. P., & Birkinshaw, M., 1998, *ApJ*, 501, 1
 Huterer, D., & Turner, M. S., 2000, *astro-ph/0012510*
 Inagaki, Y., Sugimoto, T., & Suto, Y., 1995, *PASJ*, 47, 411
 Irwin, J. A., & Bregman, J. N., 2000, *astro-ph/0003123*
 Jaffe, A. H., et al., 2000, *astro-ph/0007333*
 Jones, M. E., et al. 2001, *astro-ph/0103046*
 Kneissl, R., et al., 2001, *astro-ph/0103042*
 Komatsu, E., et al., 2001, *PASJ*, 53, 57

- Lasenby, A. N., Bridle, S. L., & Hobson, M. P., 1999, *astro-ph/9901303*
- Lauer, T. R., & Postman, M., 1994, *ApJ*, 425, 418
- Lee, A. T., et al., 2001, *astro-ph/0104459*
- Lineweaver, C., 1998, *ApJ*, in press, *astro-ph/9805326*
- Loeb, A., & Refregier, A., 1997, *ApJ*, 476, L59
- Majumdar, S., & Subrahmanyan, R., 2000, *ApJ*, 542, 597
- Maloney, P. R., & Bland-Hawthorn, J., 2001, *astro-ph/0104422*
- Mason, B., 1999, PhD Thesis, University of Pennsylvania
- Mason, B. S., Myers, S. T., & Readhead, A. C. S., 2001, *astro-ph/0101169*
- Metcalf, R. B., & Silk, J., 1998, *ApJ*, 492, L1
- Mauskopf, P. D., et al., 2000, *ApJ*, 536, L59
- Miller, A. D. et al., 1999, *ApJ*, 524, 1
- Mohr, J. J., Evrard, A. E., Fabricant, D. G., & Geller, M. J., 1995, *ApJ*, 447, 8
- Mohr, J. J., Mathiesen, B., & Evrard, A. E., 1999, *ApJ*, 517, 627
- Molnar, S. M., 2000, ASP Conference Series, eds.: Giacconi, R., Stella, L., & Serio, S.
- Molnar, S. M., & Birkinshaw, M., 1999, *ApJ*, 523, 78
- Nagai, D., Sulkanen, M. E., Evrard, A. E., 2000, *MNRAS*, 316, 120
- Peebles, P. J., 1993, "Principles of Physical Cosmology", Princeton: Princeton University Press
- Pen, U., 1997, *New Astronomy*, 2, 309
- Perlmutter, S., et al., 1999, *ApJ*, 517, 565
- Peterson, J. R., et al., 2001, *A&A*, 365, L104
- Petrosian, V., 2001, *astro-ph/0101145*
- Puy, D., Grenacher, L., Jetzer, Ph., and Signore, M., 2000, *A&A*, 363, 415
- Reese, E. D., et al., *ApJ*, 533, 38
- Rephaeli, Y., 1995, *ARA&A*, 33, 541
- Rephaeli, Y., & Yankovitch, D., 1997, *ApJ*, 481, L55
- Riess, A. G., et al. 2000, *astro-ph/0001384*
- Rizza, E., Loken, C., Bliton, M., Roettiger, K., & Burns, J., 2000, *AJ*, 119, 21
- Roettiger, K., Burns, J. O., & Pinkney, J., 1995, *ApJ*, 453, 634
- Roettiger, K., Stone, J. M., & Mushotzky, R. F., 1997, *ApJ*, 482, 588
- Sarazin, C. L., 1999, *ApJ*, 520, 529
- Sarazin, C. L., 1988, "X-ray emissions from clusters of galaxies", Cambridge University Press, Cambridge
- Sasaki, S., 1996, *PASJ*, 48, L119
- Schlickeiser, R., 1991, *A&A*, 248, L23
- Schmidt, R. W., Allen, S. W., & Fabian, A. C., 2001, *astro-ph/0107311*
- Silk, J., & White, S. D. M., 1978, *ApJ*, 226, 103
- Seljak, U., 1996, 463, 1
- Sulkanen, M. E., 1999, *ApJ*, 522, 59
- Sunyaev, R. A., & Zel'dovich, Y. B., 1980, *ARA&A*, 18, 537
- Tamura, T., et al., 2001, *ã*, 365, L87
- Tegmark, M. & Zaldarriaga, M., 2000, *astro-ph/0002091*
- Tegmark, M., Eisenstein, D. J., Hu, W., & Knor, R. G., 1998, *astro-ph/9805117*
- Tozzi, P., & Norman, C., 2000, *astro-ph/0003289*
- Turner, M. S., 2000, *Physica Scripta*, 85, 210
- Ueda, H., Itoh, M., & Suto, Y., 1993, *ApJ*, 408, 3
- White, M., 1998, *ApJ*, 506, 495
- White, R. E., & Sarazin, C. L., 1987, *ApJ*, 318, 629
- Yoshikawa, K., Itoh, M., & Suto, Y., 1998, *PASJ*, 50, 203
- Zaroubi, S., Squires, G., Hoffman, Y., & Silk, J., 1998, *ApJ*, 500, L87
- Zaldarriaga, M., Spergel, D. N., & Seljak, U., 1997, *ApJ*, 488, 1

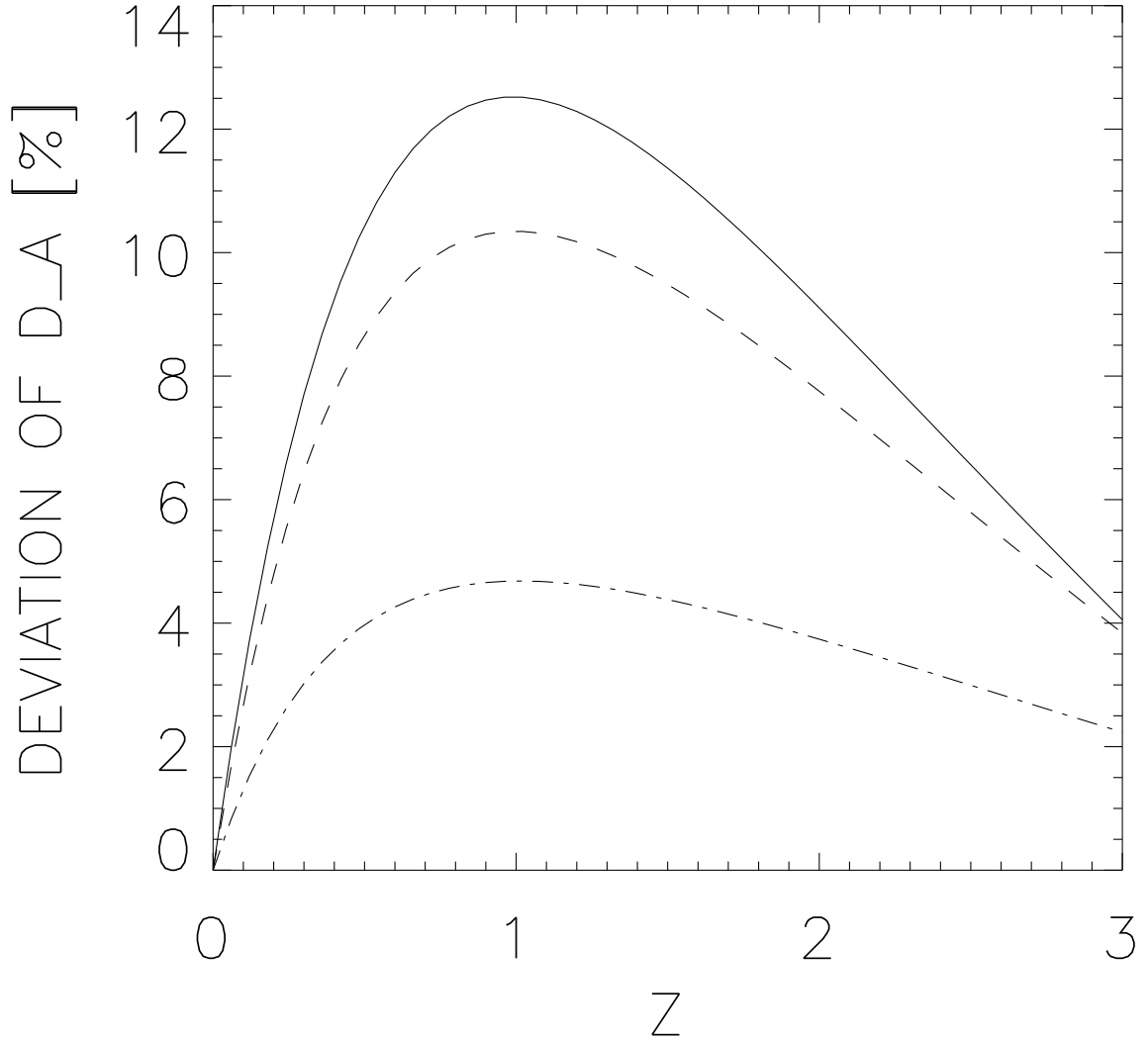


FIG. 1.— Deviation of the angular diameter distance in Universes with $\Omega_m = 0.3$ and $\Omega_\Lambda = 0.7, 0.6,$ and 0.3 relative to the angular distance function for a Universe with $\Omega_m = 0.3$ and $\Omega_\Lambda = 0$ model, as a function of z (with $h = 0.65$). The solid, short dashed, and dash dotted lines represent percentage deviations with $\Omega_\Lambda = 0.7, 0.6,$ and 0.3 respectively.

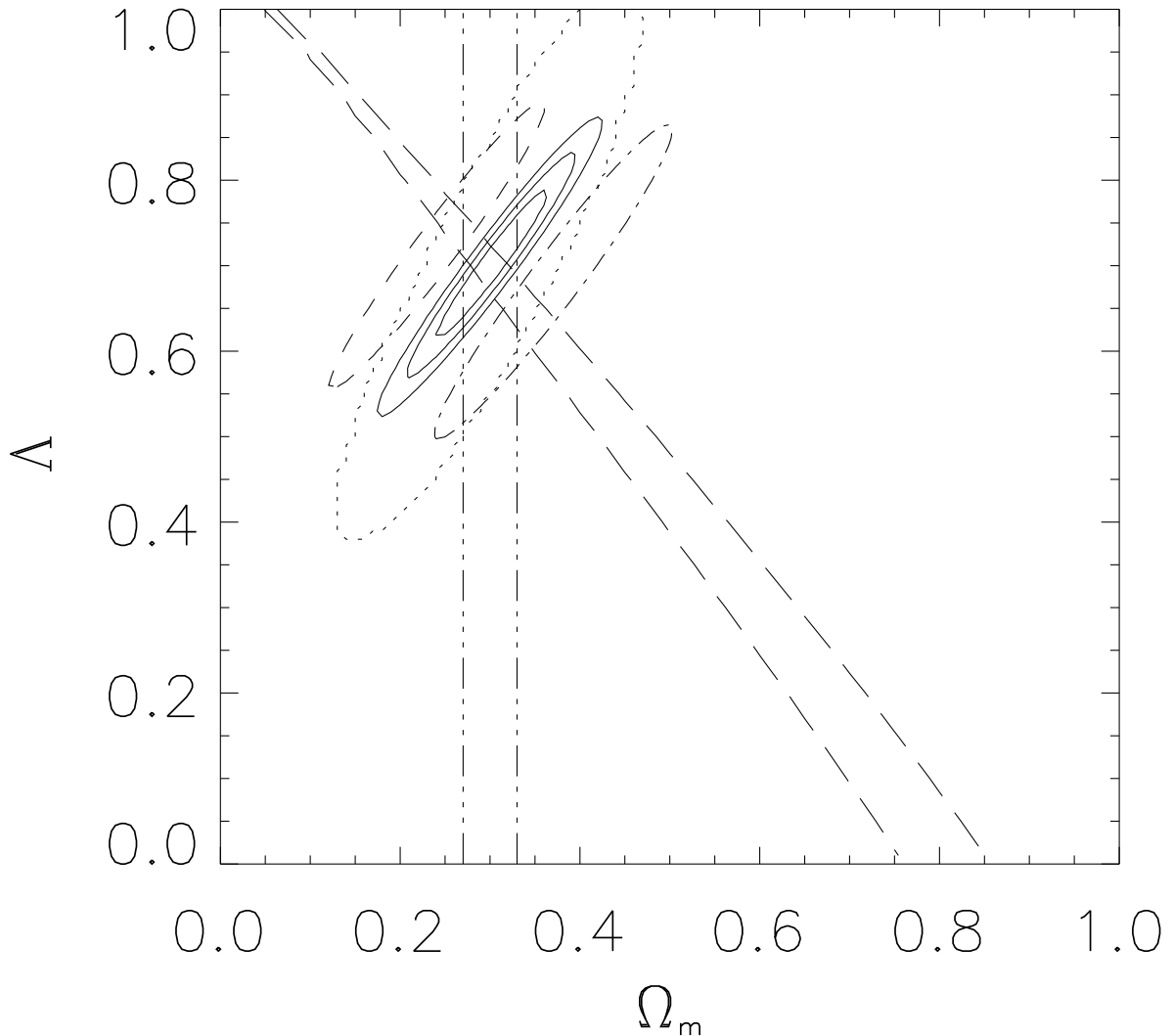


FIG. 2A.— 1, 2 and 3σ constraints on cosmological parameters from simulated angular diameter distance measurements. We used a spatially flat CDM model as a fiducial model with $\Omega_m = 0.3$, $\Omega_\Lambda = 0.7$, and $h = 0.65$. The figures show results of simulations using 500 clusters assuming a random error of 4% in the angular diameter distance (concentric solid ellipses). 2-dimensional (2D) projections of the 3D surface of 3σ constraints are shown using dotted lines. 3σ constraints assuming an additional $\pm 3\%$ systematic error are shown using solid ellipses above and below the random ellipses (Figure b and c). Constraints from a systematic error which grows from 0% to $\pm 3\%$ at $z = 1$ is shown using short dashed and dash dotted lines. Panels a, b, and c show two dimensional slices of the three dimensional parameter space defined by $(\Omega_m, \Omega_\Lambda, h)$ passing through the best-fit model as defined by the minimum of χ^2 . Constraints that might be derived from the location of the first Doppler peak, assuming $\ell_{peak} = 245 \pm 10$, are shown as long dashed lines, and define surfaces almost perpendicular to the error regions from $D_A(z)$ in the $\Omega_m - h$ plane. Constraints from $\Omega_m h^2 = \text{constant}$, assuming a 10% error in its determination from CMB experiments, are shown using dash-dot-dot lines.

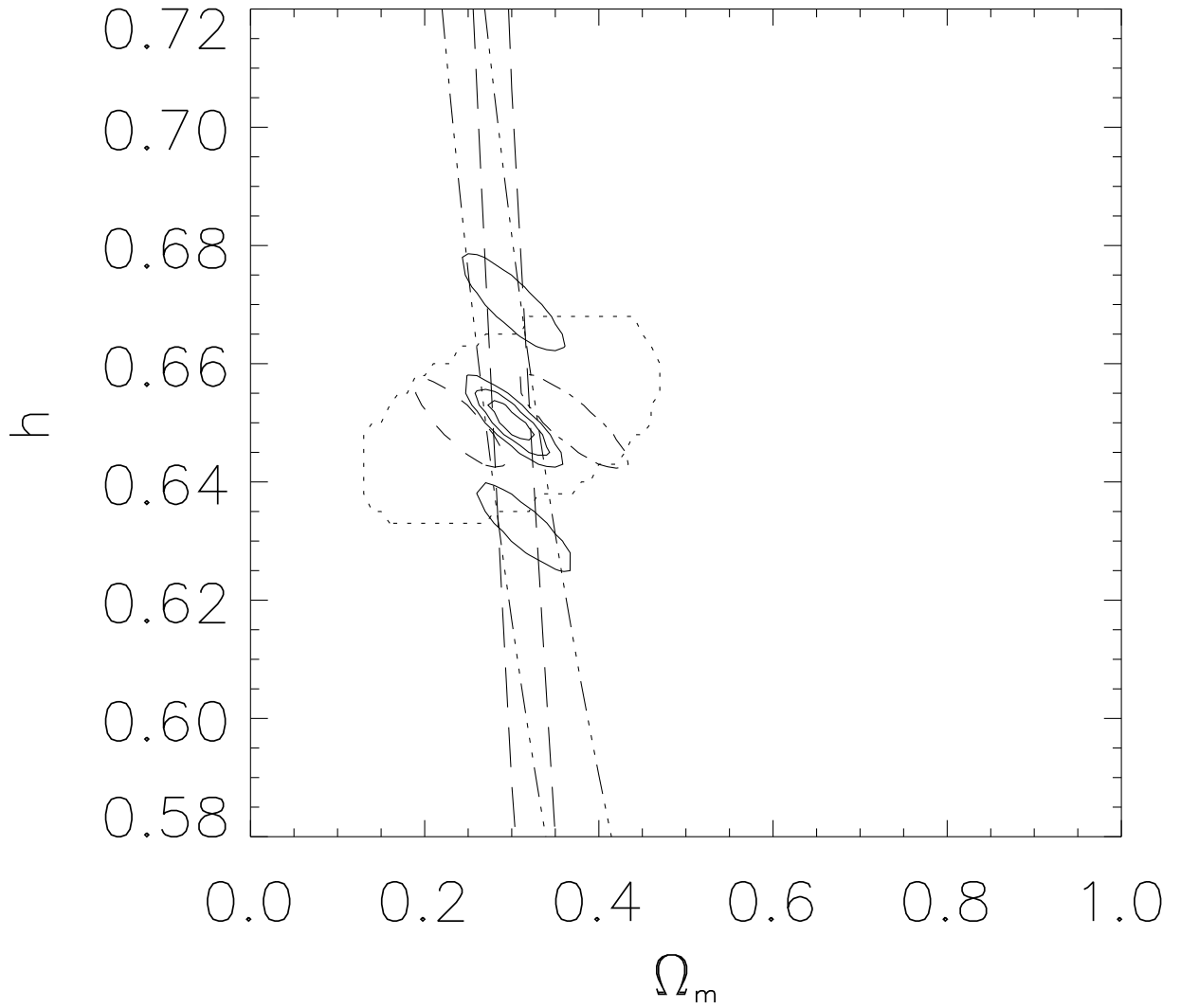


FIG. 2B.— 1, 2 and 3σ constraints on cosmological parameters from simulated angular diameter distance measurements. We used a spatially flat CDM model as a fiducial model with $\Omega_m = 0.3$, $\Omega_\Lambda = 0.7$, and $h = 0.65$. The figures show results of simulations using 500 clusters assuming a random error of 4% in the angular diameter distance (concentric solid ellipses). 2-dimensional (2D) projections of the 3D surface of 3σ constraints are shown using dotted lines. 3σ constraints assuming an additional $\pm 3\%$ systematic error are shown using solid ellipses above and below the random ellipses (Figure b and c). Constraints from a systematic error which grows from 0% to $\pm 3\%$ at $z = 1$ is shown using short dashed and dash dotted lines. Panels a, b, and c show two dimensional slices of the three dimensional parameter space defined by $(\Omega_m, \Omega_\Lambda, h)$ passing through the best-fit model as defined by the minimum of χ^2 . Constraints that might be derived from the location of the first Doppler peak, assuming $\ell_{peak} = 245 \pm 10$, are shown as long dashed lines, and define surfaces almost perpendicular to the error regions from $D_A(z)$ in the $\Omega_m - h$ plane. Constraints from $\Omega_m h^2 = \text{constant}$, assuming a 10% error in its determination from CMB experiments, are shown using dash-dot-dot lines.

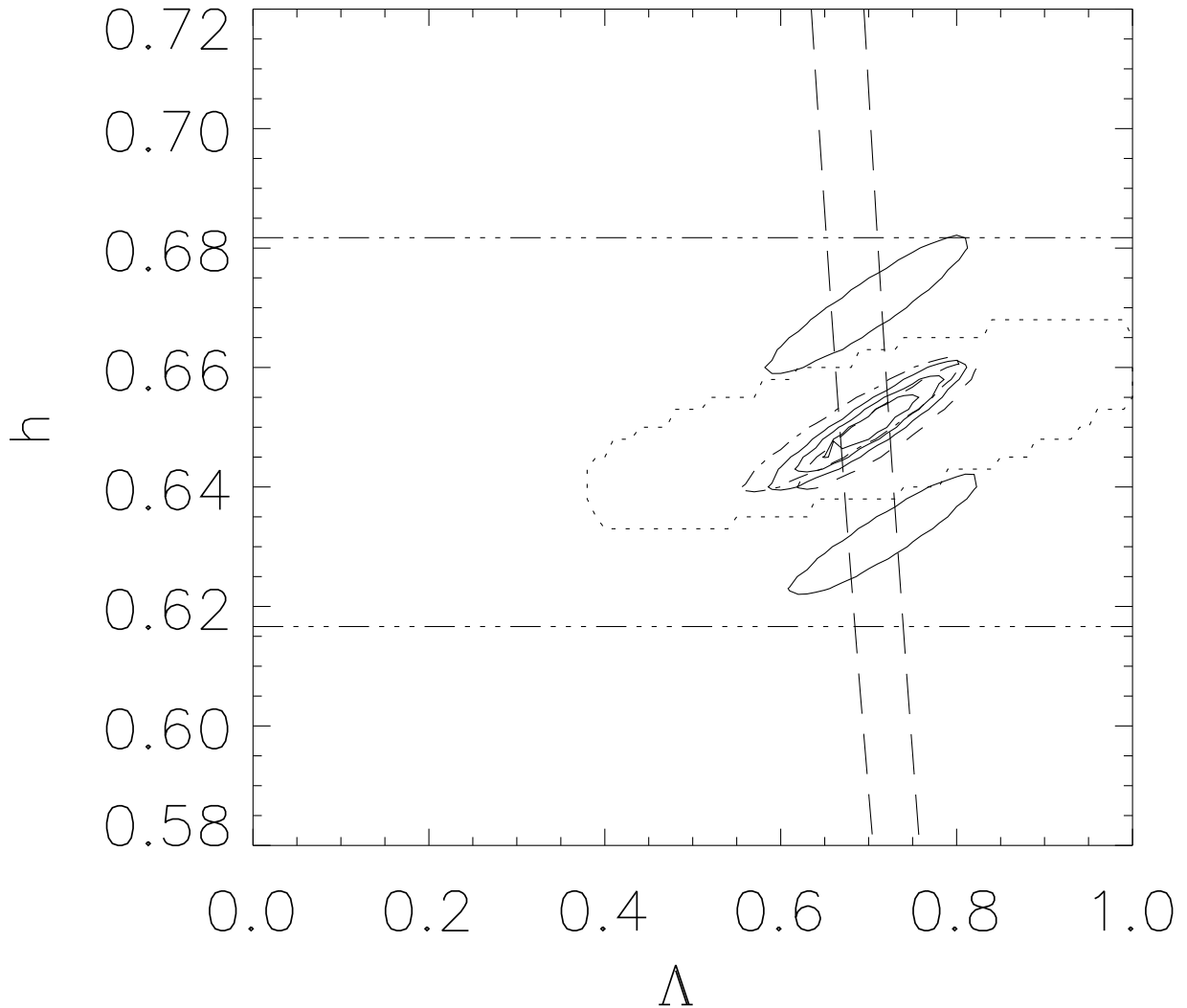


FIG. 2c.— 1, 2 and 3σ constraints on cosmological parameters from simulated angular diameter distance measurements. We used a spatially flat CDM model as a fiducial model with $\Omega_m = 0.3$, $\Omega_\Lambda = 0.7$, and $h = 0.65$. The figures show results of simulations using 500 clusters assuming a random error of 4% in the angular diameter distance (concentric solid ellipses). 2-dimensional (2D) projections of the 3D surface of 3σ constraints are shown using dotted lines. 3σ constraints assuming an additional $\pm 3\%$ systematic error are shown using solid ellipses above and below the random ellipses (Figure b and c). Constraints from a systematic error which grows from 0% to $\pm 3\%$ at $z = 1$ is shown using short dashed and dash dotted lines. Panels a, b, and c show two dimensional slices of the three dimensional parameter space defined by $(\Omega_m, \Omega_\Lambda, h)$ passing through the best-fit model as defined by the minimum of χ^2 . Constraints that might be derived from the location of the first Doppler peak, assuming $\ell_{peak} = 245 \pm 10$, are shown as long dashed lines, and define surfaces almost perpendicular to the error regions from $D_A(z)$ in the $\Omega_m - h$ plane. Constraints from $\Omega_m h^2 = \text{constant}$, assuming a 10% error in its determination from CMB experiments, are shown using dash-dot-dot lines.

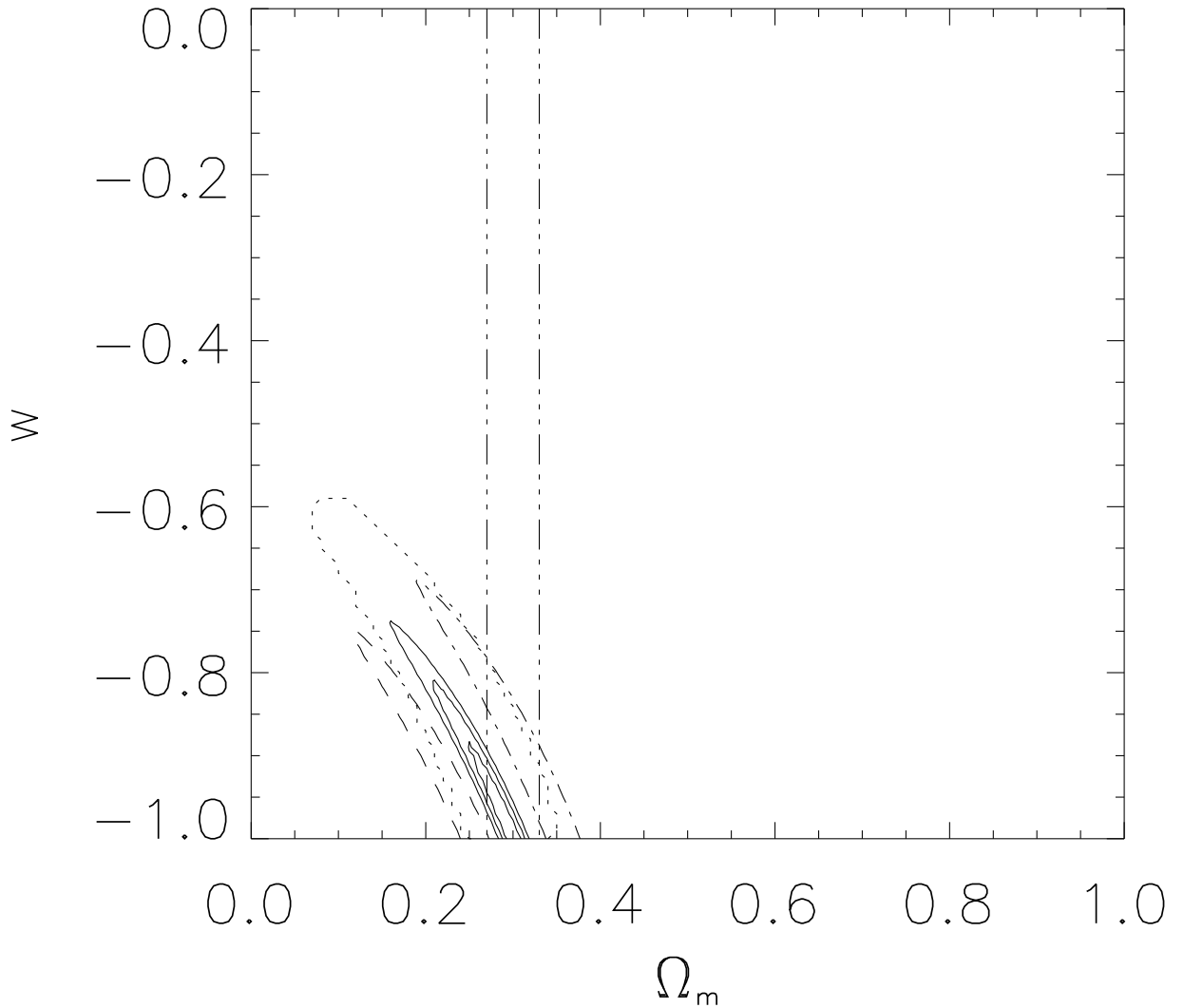


FIG. 3A.— 1, 2 and 3σ constraints on cosmological parameters from simulated angular diameter distance measurements. Contours and lines have the same meaning as in Figure 2. The figures show results of simulations using 500 clusters assuming an error of 4% in the angular diameter distance (concentric ellipses, solid lines). 3σ constraints assuming an additional $\pm 3\%$ systematic error are shown using solid ellipses above and below the random ellipses (panels b and c). Panels a, b, and c show two dimensional slices of the three dimensional parameter space defined by $(\Omega_m, w, \text{ and } h)$ and passing through the best-fit model as in Figure 2. Constraints from $\Omega_m h^2 = \text{constant}$, assuming a 10% error in its determination from CMB experiments, are shown using dash-dot-dot lines.

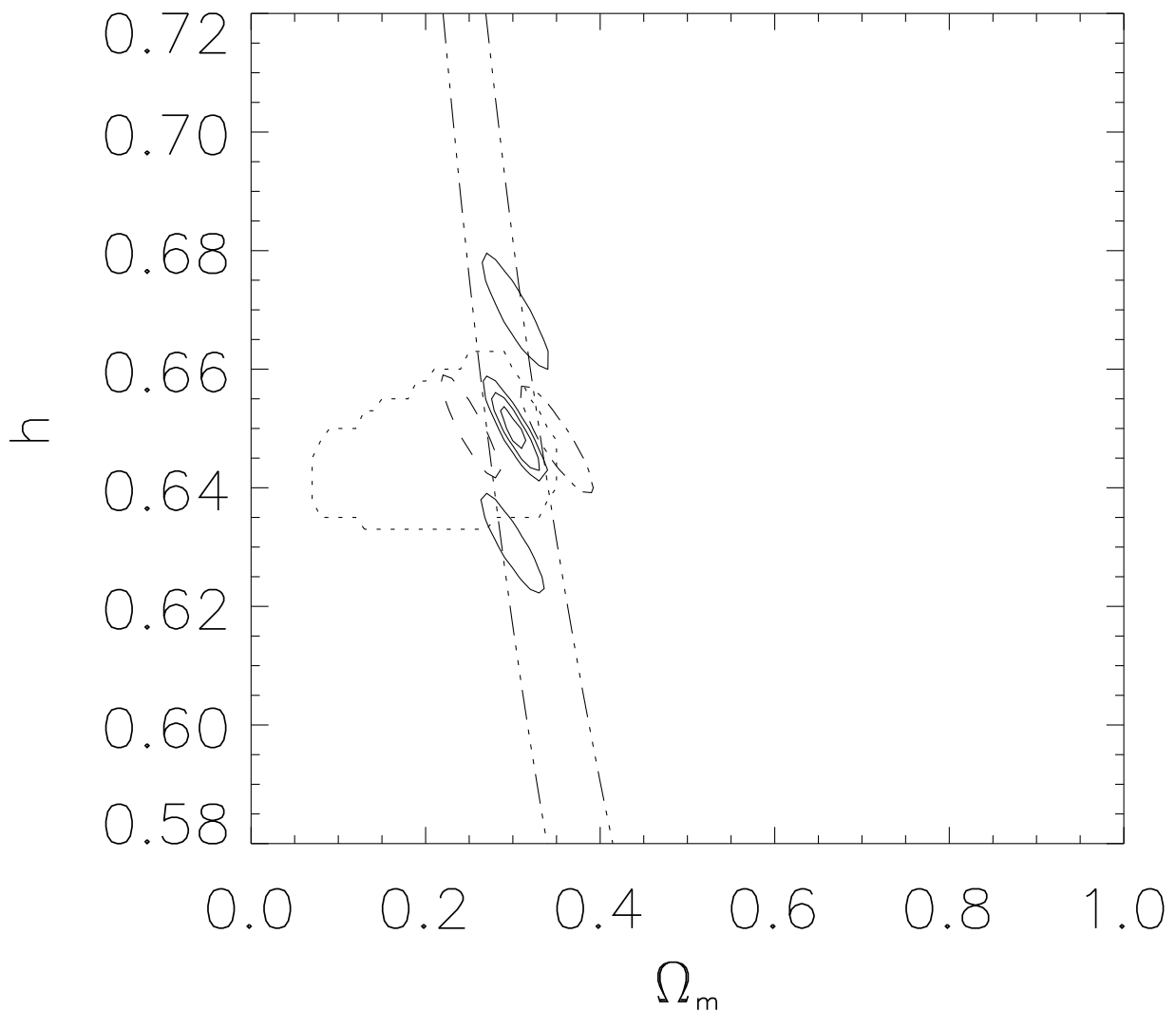


FIG. 3B.— 1, 2 and 3σ constraints on cosmological parameters from simulated angular diameter distance measurements. Contours and lines have the same meaning as in Figure 2. The figures show results of simulations using 500 clusters assuming an error of 4% in the angular diameter distance (concentric ellipses, solid lines). 3σ constraints assuming an additional $\pm 3\%$ systematic error are shown using solid ellipses above and below the random ellipses (panels b and c). Panels a, b, and c show two dimensional slices of the three dimensional parameter space defined by $(\Omega_m, w, \text{ and } h)$ and passing through the best-fit model as in Figure 2. Constraints from $\Omega_m h^2 = \text{constant}$, assuming a 10% error in its determination from CMB experiments, are shown using dash-dot-dot lines.

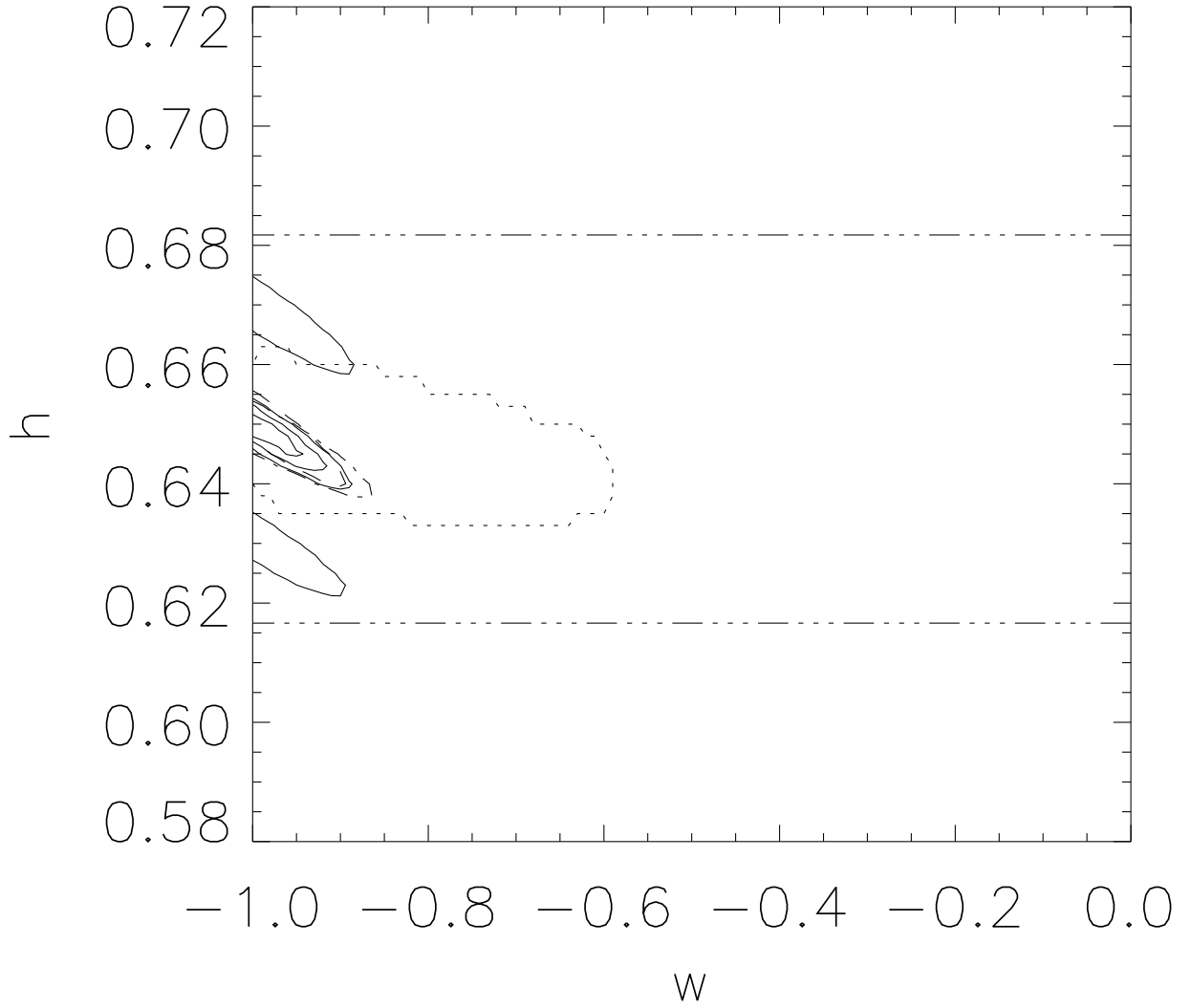


FIG. 3c.— 1, 2 and 3σ constraints on cosmological parameters from simulated angular diameter distance measurements. Contours and lines have the same meaning as in Figure 2. The figures show results of simulations using 500 clusters assuming an error of 4% in the angular diameter distance (concentric ellipses, solid lines). 3σ constraints assuming an additional $\pm 3\%$ systematic error are shown using solid ellipses above and below the random ellipses (panels b and c). Panels a, b, and c show two dimensional slices of the three dimensional parameter space defined by $(\Omega_m, w, \text{ and } h)$ and passing through the best-fit model as in Figure 2. Constraints from $\Omega_m h^2 = \text{constant}$, assuming a 10% error in its determination from CMB experiments, are shown using dash-dot-dot lines.

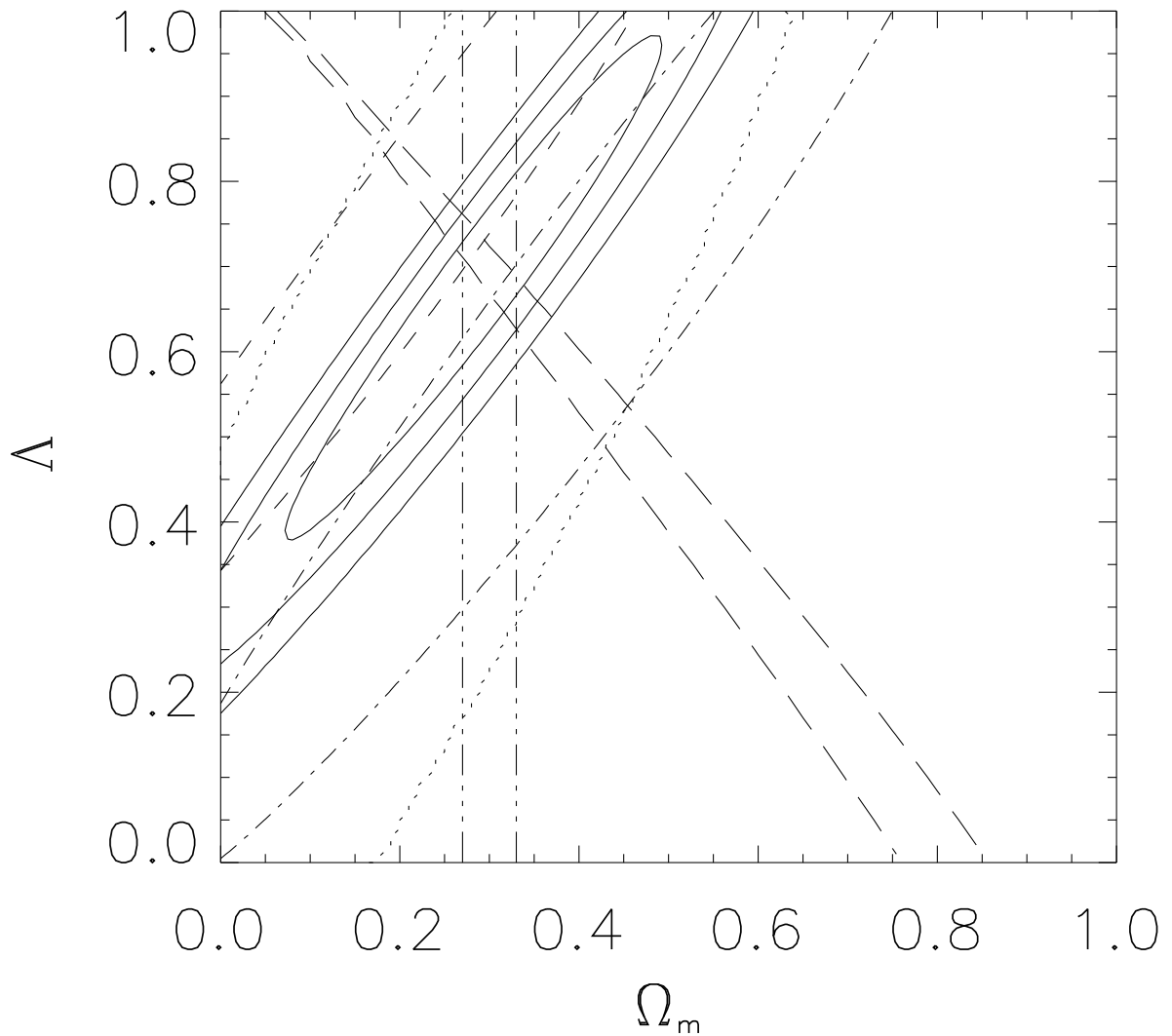


FIG. 4A.— Same as Figure 2, but with only 70 clusters (with 35 at $z > 0.5$) assuming a 7% random error in the angular diameter distances. We omit the redshift-independent systematic error ellipses, since they simply correspond to the same shifts on the h axis seen in Fig. 2, but retain the redshift-dependent systematic error ellipses corresponding to a 5% gradient in the error in D_A .

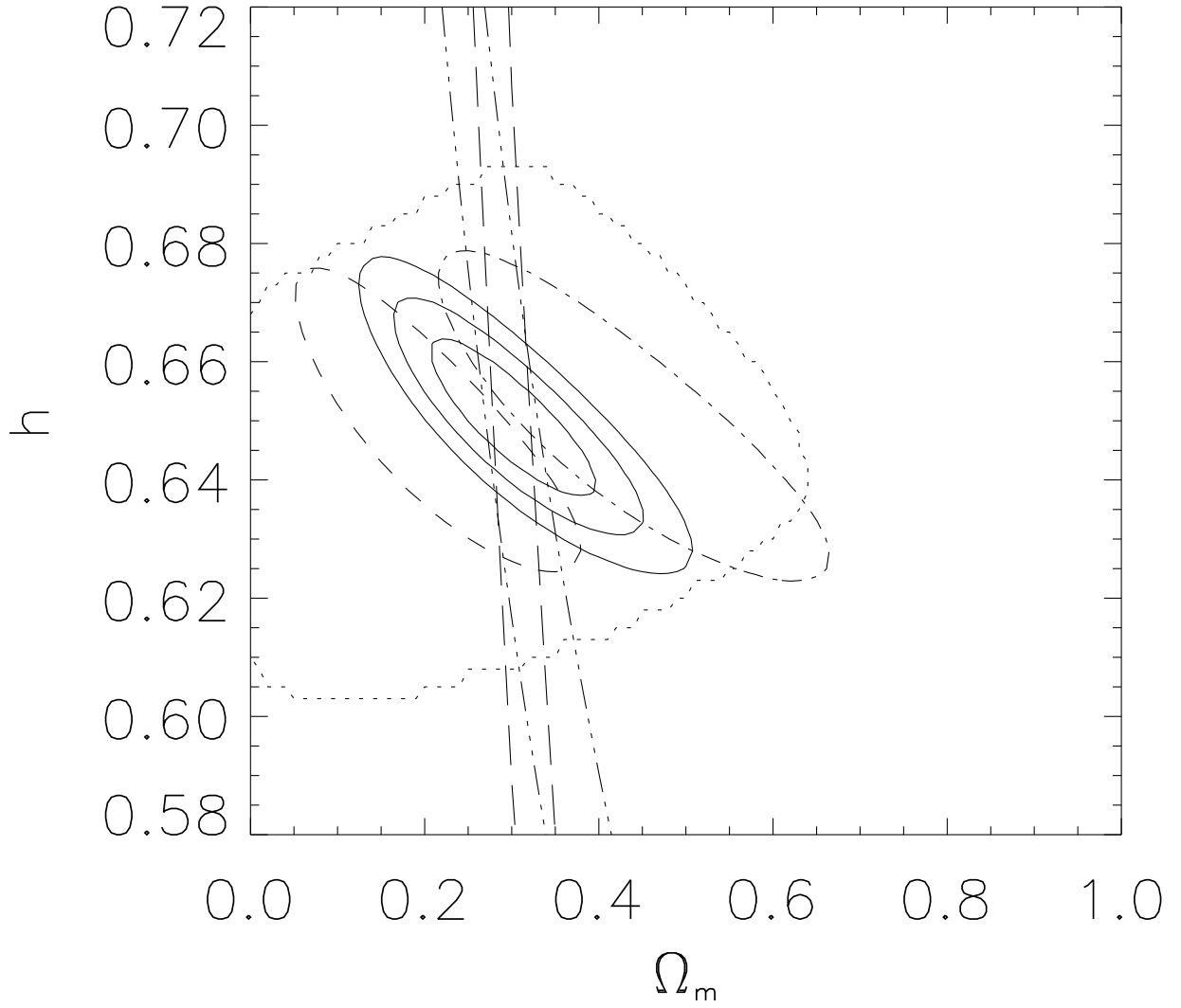


FIG. 4B.— Same as Figure 2, but with only 70 clusters (with 35 at $z > 0.5$) assuming a 7% random error in the angular diameter distances. We omit the redshift-independent systematic error ellipses, since they simply correspond to the same shifts on the h axis seen in Fig. 2, but retain the redshift-dependent systematic error ellipses corresponding to a 5% gradient in the error in D_A .

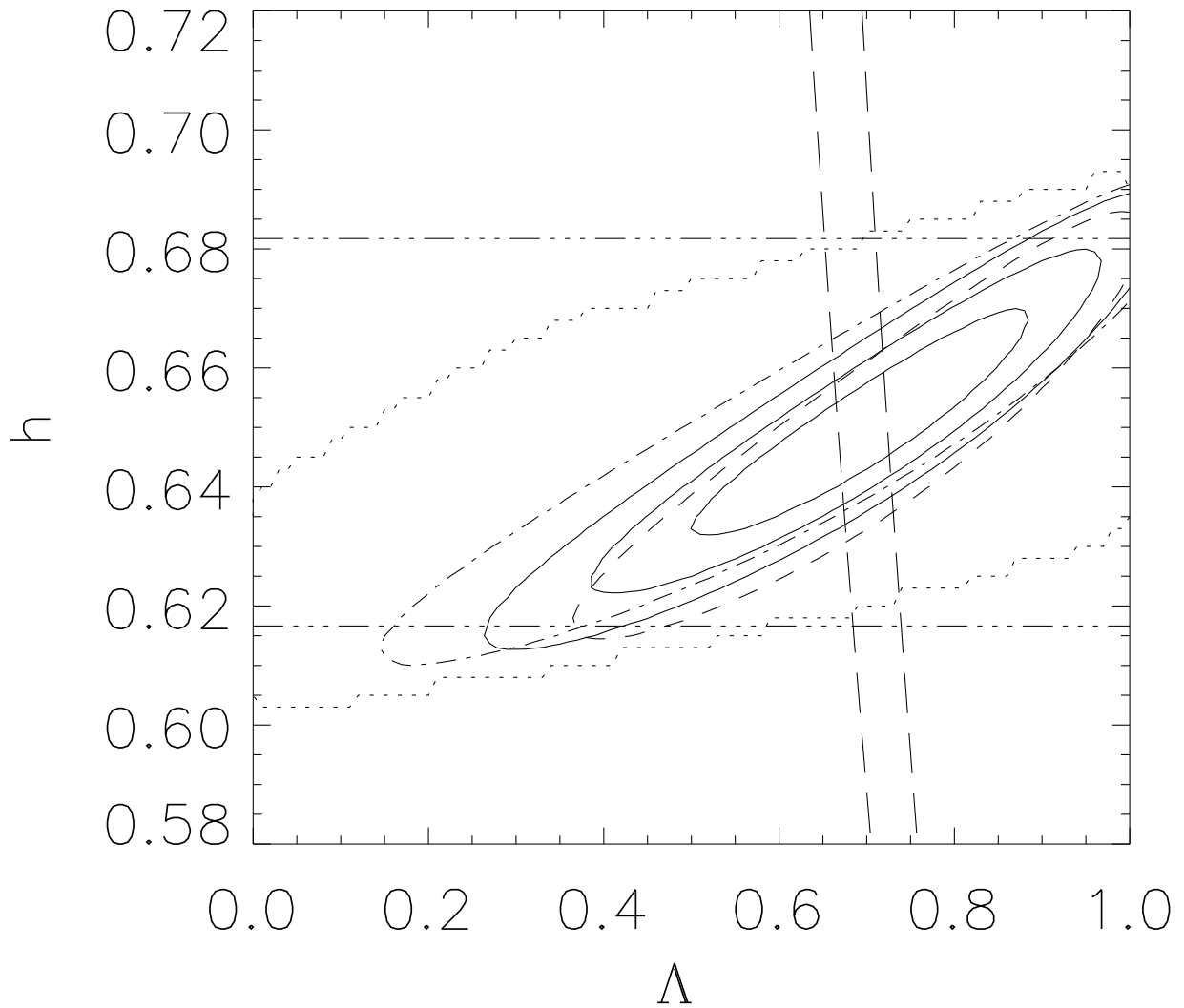


FIG. 4C.— Same as Figure 2, but with only 70 clusters (with 35 at $z > 0.5$) assuming a 7% random error in the angular diameter distances. We omit the redshift-independent systematic error ellipses, since they simply correspond to the same shifts on the h axis seen in Fig. 2, but retain the redshift-dependent systematic error ellipses corresponding to a 5% gradient in the error in D_A .

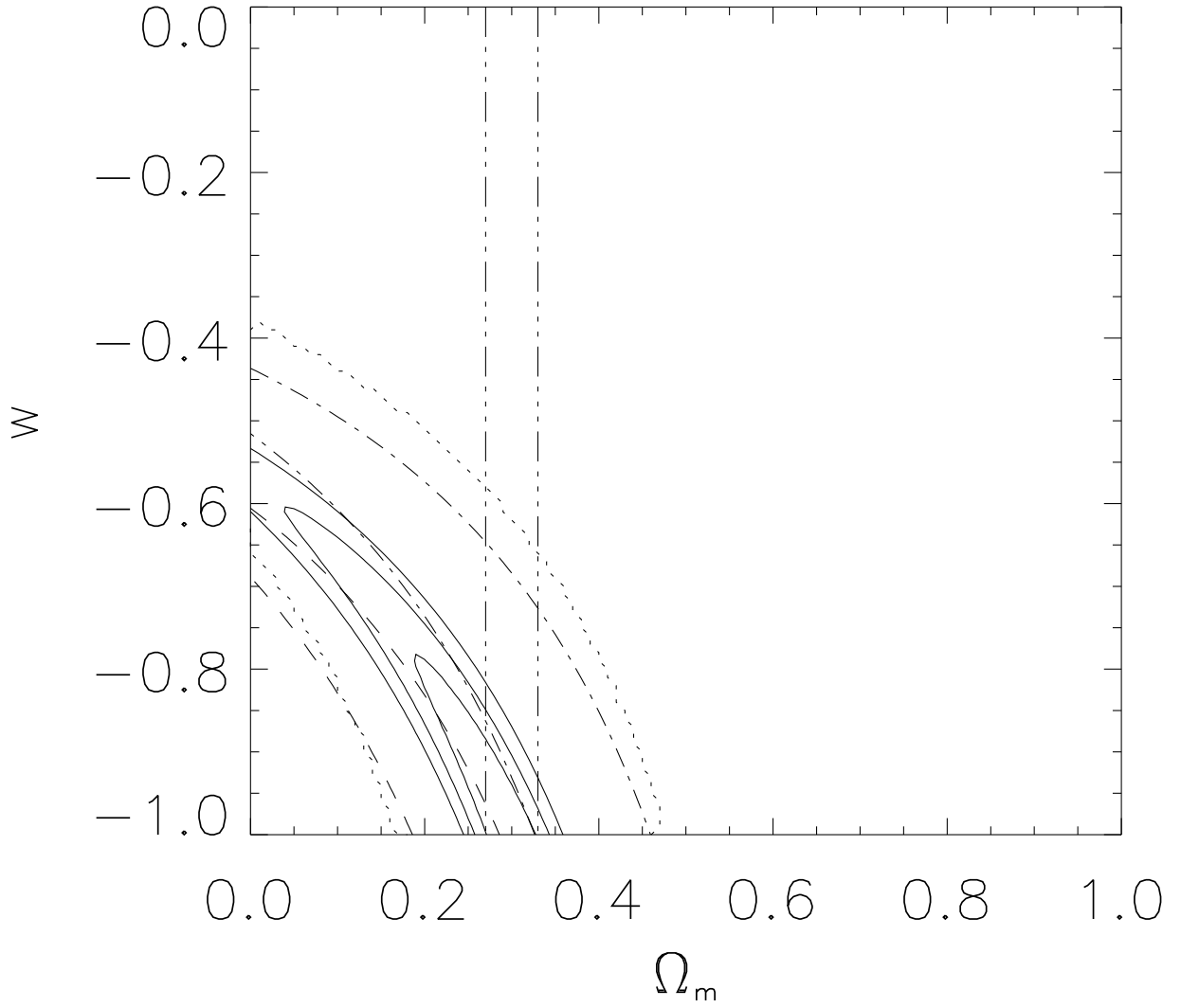


FIG. 5A.— Same as Figure 3, but with only 70 clusters (with 35 at $z > 0.5$) assuming a 7% random error in the angular diameter distances. We omit the redshift-independent systematic error ellipses, since they simply correspond to the same shifts on the h axis seen in Fig. 2, but retain the redshift-dependent systematic error ellipses corresponding to a 5% gradient in the error in D_A .

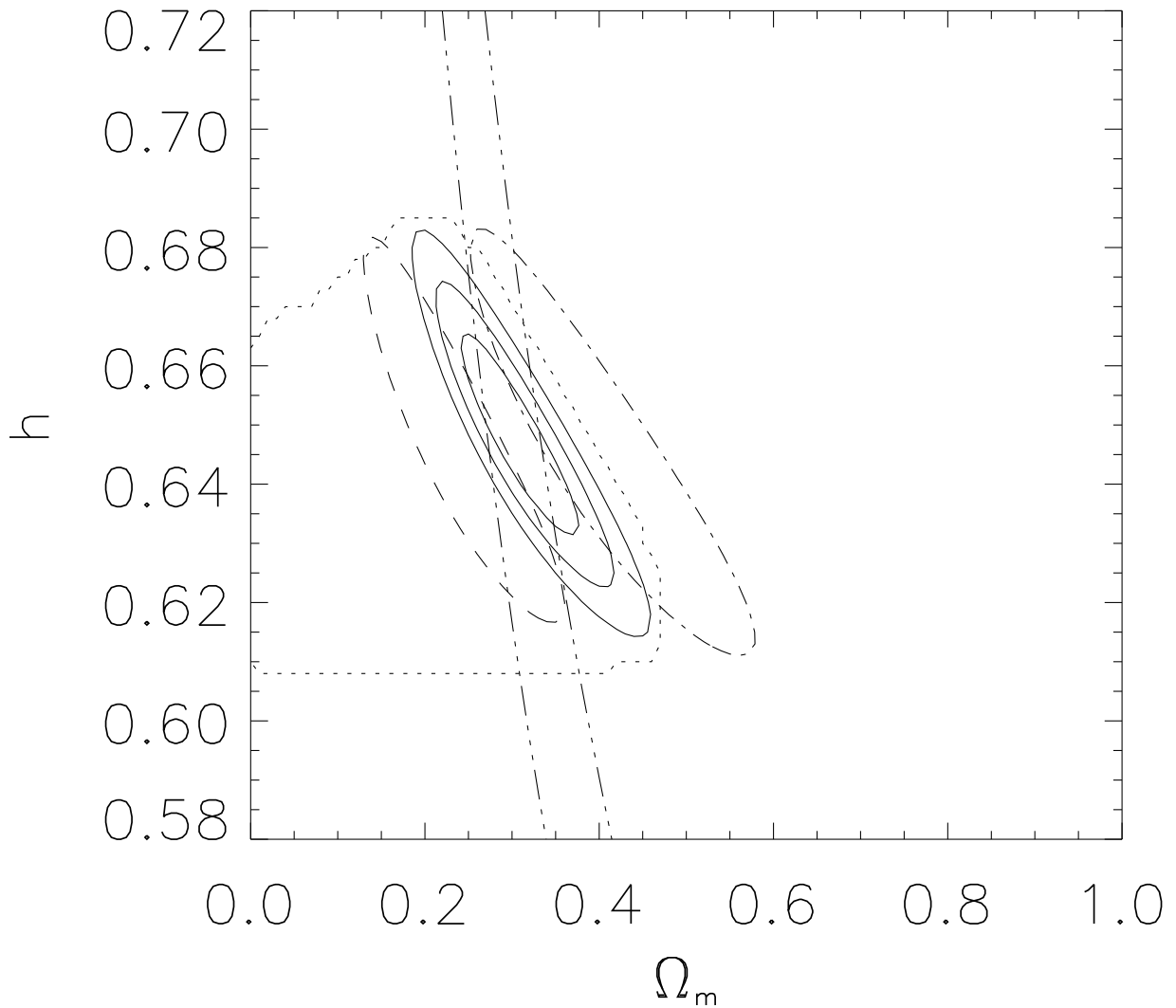


FIG. 5B.— Same as Figure 3, but with only 70 clusters (with 35 at $z > 0.5$) assuming a 7% random error in the angular diameter distances. We omit the redshift-independent systematic error ellipses, since they simply correspond to the same shifts on the h axis seen in Fig. 2, but retain the redshift-dependent systematic error ellipses corresponding to a 5% gradient in the error in D_A .

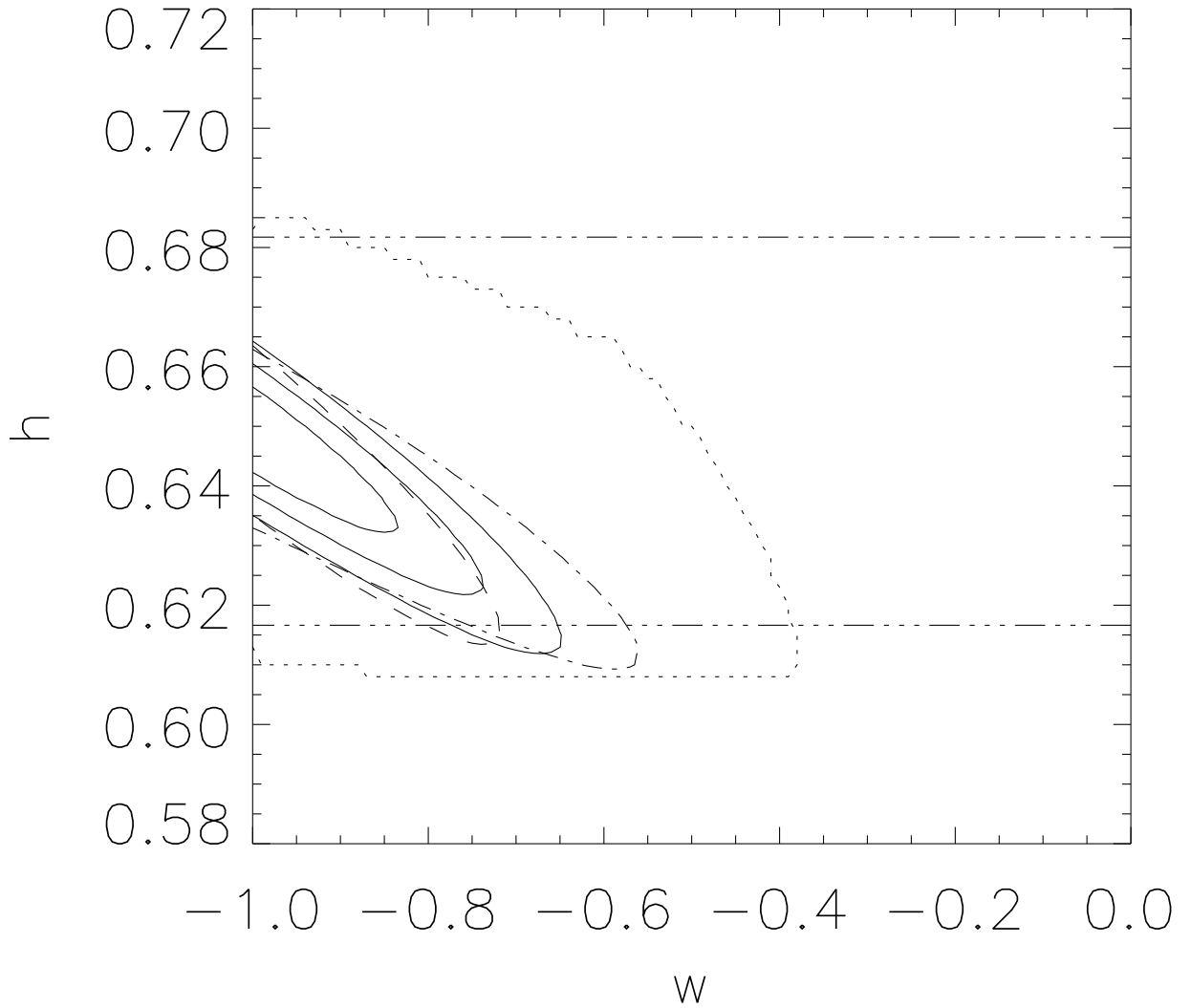


FIG. 5C.— Same as Figure 3, but with only 70 clusters (with 35 at $z > 0.5$) assuming a 7% random error in the angular diameter distances. We omit the redshift-independent systematic error ellipses, since they simply correspond to the same shifts on the h axis seen in Fig. 2, but retain the redshift-dependent systematic error ellipses corresponding to a 5% gradient in the error in D_A .